Emerging Device Applications for Semiconducting Two-Dimensional Transition Metal Dichalcogenides

Deep Jariwala,[†] Vinod K. Sangwan,[†] Lincoln J. Lauhon,[†] Tobin J. Marks,[†,‡] and Mark C. Hersam[†,‡,§,*]

[†]Department of Materials Science and Engineering, [‡]Department of Chemistry, and [§]Department of Medicine, Northwestern University, Evanston, Illinois 60208, United States

ABSTRACT With advances in exfoliation and synthetic techniques, atomically thin films of semiconducting transition metal dichalcogenides have recently been isolated and characterized. Their two-dimensional structure, coupled with a direct band gap in the visible portion of the electromagnetic spectrum, suggests suitability for digital electronics and optoelectronics. Toward that end, several classes of high-performance devices have been reported along with significant progress in understanding their physical properties. Here, we present a review of the architecture, operating principles, and physics of electronic and optoelectronic devices based on ultrathin transition metal dichalcogenide semiconductors. By critically assessing and comparing the performance of these devices with competing technologies, the merits and shortcomings of this emerging class of electronic materials are identified, thereby providing a roadmap for future development.

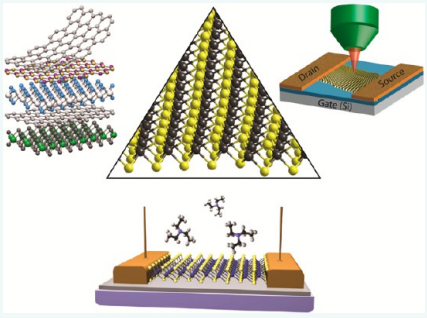

KEYWORDS: molybdenum disulfide · digital electronics · field-effect transistor · van der Waals heterostructure · nanoelectronics · optoelectronics · flexible electronics · valleytronics · photodetector · photovoltaic · solar cell · light-emitting diode · sensor

The relentless miniaturization of silicon-based electronics coupled with the advent of graphene has led the electronic materials community toward atomically thin two-dimensional semiconductors.[1] While graphene has attracted significant attention, it lacks a band gap and thus is unsuitable for digital electronic applications.[1−5] Consequently, significant effort has been devoted to identifying alternative two-dimensional semiconductors. Several classes of non-graphene-layered compounds have received recent attention including boron nitride, metal chalcogenides, oxides, hydroxides, and oxychlorides. A comprehensive list of all known layered van der Waals solids has been reported in a number of recent reviews.[6−11] However, only a few of these layered materials can be classified as semiconductors, and even fewer have been successfully isolated as air-stable, high-quality, two-dimensional crystals.

Transition metal dichalcogenides (TMDCs) are among the most studied layered compounds that have been isolated in monolayer form. Compounds in the TMDC family exhibit a wide range of electrical properties, depending on polytype and the number of transition metal d-electrons, and include metallic,[12] half-metallic,[13] semiconducting,[14−16] superconducting,[17] and charge density wave[18] behavior. In particular, molybdenum- and tungsten-based TMDCs are semiconductors with band gaps ranging from the visible to the near-infrared. Besides Mo and W, chalcogenides of Ti, Sn, and Zr are also predicted to be semiconducting, but little to no experimental evidence exists on their isolation in monolayer form, stability, or performance in devices.[19−23] Thus, Mo and W chalcogenides have been the most heavily investigated among the post-graphene two-dimensional materials.

This review will primarily focus on semiconducting TMDCs based on Mo and W and their applications in devices. First, the unique physical properties of semiconducting TMDCs that are most relevant in device applications will be highlighted such as crystal structure, symmetry, the thickness-dependent evolution of electronic and phonon structure, as well as the effects of

* Address correspondence to m-hersam@northwestern.edu.

Received for review January 6, 2014 and accepted January 29, 2014.

Published online January 29, 2014
10.1021/nn500064s

quantum confinement. A series of emerging electronic and optoelectronic device applications will then be delineated, including field-effect transistors (FETs), heterostructure junctions, photodetectors, photovoltaics, and sensors. In order to provide context and identify the most productive opportunities for future research, TMDC device metrics will be compared and contrasted with those of competing semiconductors and pre-existing technologies.[3,24−33]

Physical Properties. TMDCs have the chemical formula MX_2, where M is a transition element and X is a chalcogen.[12,34,35] Various permutations of these elements result in over 40 different compounds, although not all of them are layered solids.[6,8,12,36] A monolayer is defined here as a hexagonally ordered plane of metal atoms sandwiched between two hexagonally ordered planes of chalcogen atoms, where the formal oxidation states of the metal and chalcogen elements are +4 and −2, respectively.[35] The structure of layered TMDCs is similar to that of graphite, and each layer has a thickness of 6−7 Å with strong in-plane covalent bonding and weak out-of-plane van der Waals interactions (Figure 1a). Bulk TMDCs are found in several structural polytypes depending on the stacking order of the layers,[35] while single layers of TMDCs are found in two polytypes, depending on the position of the chalcogen with respect to the metal element in the X−M−X structure. The TMDC monolayer polytypes can be either trigonal prismatic (D_{3h} point group, honeycomb motif) or octahedral (D_{3d} point group, centered-honeycomb motif) also referred to as 2H (1H for a monolayer) and 1T, respectively (Figure 1b).[8,35,37] The half-filled d-orbitals of group VIB transition metals (*i.e.*, M = Cr, Mo, W) results in semiconducting behavior with decreasing band gap as the chalcogen atomic number is increased (*i.e.*, X = S, Se, Te). These semiconducting TMDCs are found primarily as the 2H polytype, although reversible transitions to the 1T polytype have been achieved *via* chemical processing.[38]

VOCABULARY: **mobility** - a term used to characterize the speed of electric charge carriers upon application of an electric field; **field-effect transistor** - a three-terminal electronic device that functions as a voltage-controlled switch; **diode** - an electronic device with highly asymmetric current−voltage characteristics that predominantly allows current flow for only one bias polarity; **van der Waals heterostructure** - vertical stack of disparate two-dimensional materials interacting only *via* weak van der Waals forces; **photodetector** - an optoelectronic device that produces electrical current in response to optical excitation

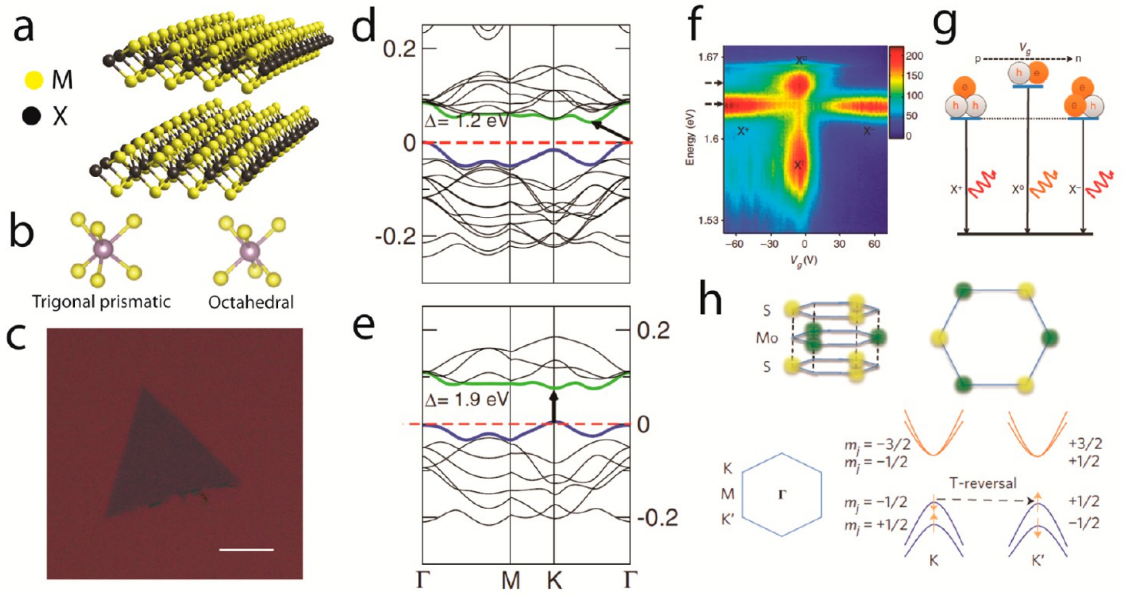

Figure 1. Physical properties of layered semiconducting transition metal dichalcogenides (TMDCs). (a) Chemical structure of two layers of a TMDC where M is a transition element and X is a chalcogen. (b) Two polytypes of single-layer TMDCs: trigonal prismatic (1H) and octahedral (1T). Adapted with permission from ref 8. Copyright 2013 Macmillan Publishers Ltd. (c) Optical micrograph of single-layer MoS_2 on a 300 nm SiO_2/Si substrate (scale bar = 20 μm). (d) Band structure of bulk MoS_2 and (e) single-layer MoS_2 as calculated from density functional theory. Adapted with permission from ref 46. Copyright 2011 American Physical Society. (f) Photoluminescence energy of single-layer $MoSe_2$ plotted as a function of gate voltage. At zero gate voltage, there are neutral (X^0) and impurity-trapped excitons (X^l). With large electron and hole doping, charged excitons (trions) dominate the spectrum. (g) Schematic of a gate-dependent transition of a positive trion (X^+) to a neutral exciton and then to a negative trion (X^-). Adapted with permission from ref 56. Copyright 2013 Macmillan Publishers Ltd. (h) Top: Honeycomb lattice of single-layer MoS_2 where alternating corners are occupied by one Mo and two S atoms, resulting in broken spatial inversion symmetry. Bottom: Conduction band minima and valence band maxima are shown with corresponding *z*-components of their total angular momentum. The valence bands are split due to strong spin−orbit coupling. Adapted with permission from ref 64. Copyright 2012 Macmillan Publishers Ltd.

Weak van der Waals interactions between MX_2 layers facilitate isolation of single layers *via* mechanical[39−41] or chemical exfoliation.[6,22,23,42,43] For example, Figure 1c shows an optical image of single-layer (SL) MoS_2 exfoliated *via* the "Scotch-tape" method. The electrical properties of semiconducting TMDCs also depend on the number of layers due to quantum confinement effects and changes in symmetry.[44,45] Several groups have predicted[46−49] and verified[38,44,45,50] the transition from an indirect band gap at the Γ-point to a direct band gap at the K-point of the Brillouin zone as the semiconducting TMDC thickness is reduced to a single layer. In particular, bulk MoS_2 has an indirect band gap of 1.2 eV, whereas single-layer MoS_2 has a direct band gap of 1.9 eV (Figure 1d,e)[46] that results in enhanced photoluminescence (PL) by up to 4 orders of magnitude.[44] Similar evidence for a direct band gap transition has also been reported for single-layer $MoSe_2$, WS_2, and WSe_2.[51,52]

Recent theoretical work[49,53,54] and experiments[55−57] also suggest that optical transitions in ultrathin TMDC samples are dominated by excitons rather than direct interband transitions. For example, the optical absorption spectra of both single-layer and bilayer MoS_2 exhibit two distinct peaks that have been assigned to A and B excitons.[44] The excition binding energy is predicted to be as high as 0.5−0.9 eV for a monolayer and ∼0.4 eV for a bilayer.[49,53,54] The exciton binding energy is dependent on the strain and surrounding dielectric environment, which can be detected as shifts in the emission peak.[58−60] Furthermore, gate-dependent photoluminescence measurements on single-layer semiconducting TMDCs suggest that an exciton can be charged with an extra electron or hole to form trions (Figure 1f,g).[55,56] In addition, the unique symmetry of semiconducting TMDCs suggests promise for using a new state variable (*i.e.*, valley quantum numbers) for logic operations in so-called valleytronic devices.[61] Earlier, the valley degree of freedom had only been accessed by applying stain[62] or magnetic fields[63] in non-TMDC materials, whereas, as discussed below, the properties of TMDCs allow access to valley degrees of freedom *via* circularly polarized light. In contrast to graphene, single-layer TMDCs have a honeycomb structure with M and X_2 atoms at alternating corners, so the degeneracy of the K- and K′-points is lifted.[35,61,64] Furthermore, time reversal symmetry requires that split valleys have charge carriers with opposite spin. The net result is coupling between the spin and valley degrees of freedom, allowing confinement of charge carriers in a particular valley (Figure 1h).[61,64] Recently, multiple groups have demonstrated selective valley population by exciting edge electrons with circularly polarized light in monolayers of MoS_2 and WSe_2.[64−68]

The phonon structure of semiconducting TMDCs is also sensitive to the number of layers and strain as well as temperature and carrier concentration. The Raman spectra of TMDCs contain two predominant and distinct peaks: (1) the out-of-plane A_{1g} mode where the top and bottom X atoms are moving out of plane in opposite directions while M is stationary; (2) the in-plane degenerate $E_{2g}{}^1$ mode where the M and X atoms are moving in-plane in opposite directions.[69] The addition of extra layers leads to stiffening of the out-of-plane phonon modes and relaxation of in-plane bonding, resulting in a blue shift of the A_{1g} mode and a red shift of the $E_{2g}{}^1$ mode.[69,70] Both of these modes undergo a red shift as well as spectral broadening with increasing temperatures that is attributed to anharmonic contributions to the interatomic potentials.[71−73] The A_{1g} mode is also sensitive to carrier density and undergoes a red shift as well as peak broadening with electron doping, while the $E_{2g}{}^1$ mode remains insensitive to doping, suggesting stronger electron−phonon coupling with the out-of-plane vibrational mode.[74] The same effect is also evident in resonant Raman spectra of TMDCs where the intensity of the A_{1g} mode is greatly enhanced under resonance conditions while the enhancement vanishes with reduced thickness due to reduced electron−A_{1g} coupling in thinner samples.[70] Resonance conditions have also led to the observation of a new second-order longitudinal acoustic (LA) phonon mode, the intensity of which increases upon reduction in the sample thickness.[70,75] While the $E_{2g}{}^1$ mode remains insensitive to doping, it is very sensitive to applied strain. Applying uniaxial strain lifts the degeneracy of the $E_{2g}{}^1$ mode, leading to red shifting and splitting into two distinct peaks for strain of just 1%.[59] The unique electronic band structure and lattice vibration properties of TMDCs suggest new opportunities for electronic, optoelectronic, and sensing devices as will be outlined below.

Digital Electronic Devices. Digital electronics requires the reliable creation, storage, and reading of distinct voltage states. In Boolean logic, two states are required, corresponding to true "1" or false "0". Digital electronic circuits comprise large assemblies of logic gates, which are electronic implementations of the Boolean logic functions. Each logic gate typically consists of several transistors, making the transistor the fundamental component of modern digital electronics. Most digital electronic circuits use the metal-oxide−semiconductor field-effect transistor (MOSFET) as the basic component. The two discrete voltage states described above can be achieved by having two distinct states of conductance in a MOSFET separated by multiple orders of magnitude. This high on/off-current ratio requirement is most easily achieved at room temperature in semiconducting materials with band gaps greater than ∼1 eV. The substantial band gaps of semiconducting TMDCs suggest that high on/off-current ratios can be achieved, unlike in gapless graphene,

and thus digital electronics based on 2D materials is possible. This section will first focus on the development of ultrathin semiconducting TMDC-based FETs, followed by a review of advanced digital circuit elements such as inverters and logic gates.

Field-Effect Transistors. Although the electrical properties of bulk semiconducting TMDCs have been investigated for decades,[15,76] they were first used in FETs only over the past ~10 years.[77] It was only after the landmark paper on graphene by the Manchester group[78] that monolayers of semiconducting TMDCs were investigated in FETs.[39] In early work, the field-effect mobility for single-layer MoS_2 was found to be at least 3 orders of magnitude lower than that of graphene.[39] The interest in monolayer semiconducting TMDC FETs was renewed in 2011 when top-gated SL-MoS_2 FETs (Figure 2a inset) with moderate mobilities (~60−70 cm^2/Vs[79−81]), large on/off ratios (~10^8), and low subthreshold swings (74 mV/dec) were demonstrated at room temperature (Figure 2a).[16] The two-dimensional channel coupled with a large band gap (>1 eV) and ultrathin top gate dielectric allowed superior gate control, thus enabling small off-currents and large switching ratios. This work also suggested that the presence of the top dielectric enhanced the carrier mobility.

Since charge carriers in ultrathin TMDCs are weakly screened, the carrier mobility is sensitive to the interfaces on both sides of the semiconductor film. This effect is particularly evident in vacuum *versus* ambient measurements[82−84] of unencapsulated SL-MoS_2 FETs (Figure 2b). A significant negative shift in threshold voltage and higher on-currents are observed under vacuum conditions, indicating p-type doping and charge scattering caused by atmospheric adsorbates.[82] This performance degradation due to adsorbate interaction is reversible in the case of TMDCs by reinserting the devices into vacuum conditions unlike in organic semiconductors where this degradation is irreversible. Similarly, large mobility differences have been observed in bare *versus* top dielectric encapsulated devices,[16,80,85−87] bottom-gated devices on different dielectrics,[88−92] and prebias *versus* postbias stressing.[93] In addition, electrical double-layer gating using ion gels led to ambipolar transport[85,94,95] in otherwise n-type MoS_2 and WS_2 FETs and increased carrier mobilities *via* increased screening of charged impurities. The ambipolar behavior has been attributed to the ultrahigh capacitance of the electrical double layer, which allows tuning of the Fermi level across the band gap to allow carrier injection into both the valence band and conduction band (Figure 2c).[94] Mobility increases have also been observed with increasing TMDC thickness due to screening of charged substrate impurities in addition to accessing the third dimension for charge transport.[88,96−99] Therefore, to date, few-layer samples have exhibited the highest room temperature mobility values (>100 cm^2/Vs) in TMDC FETs.[88,100]

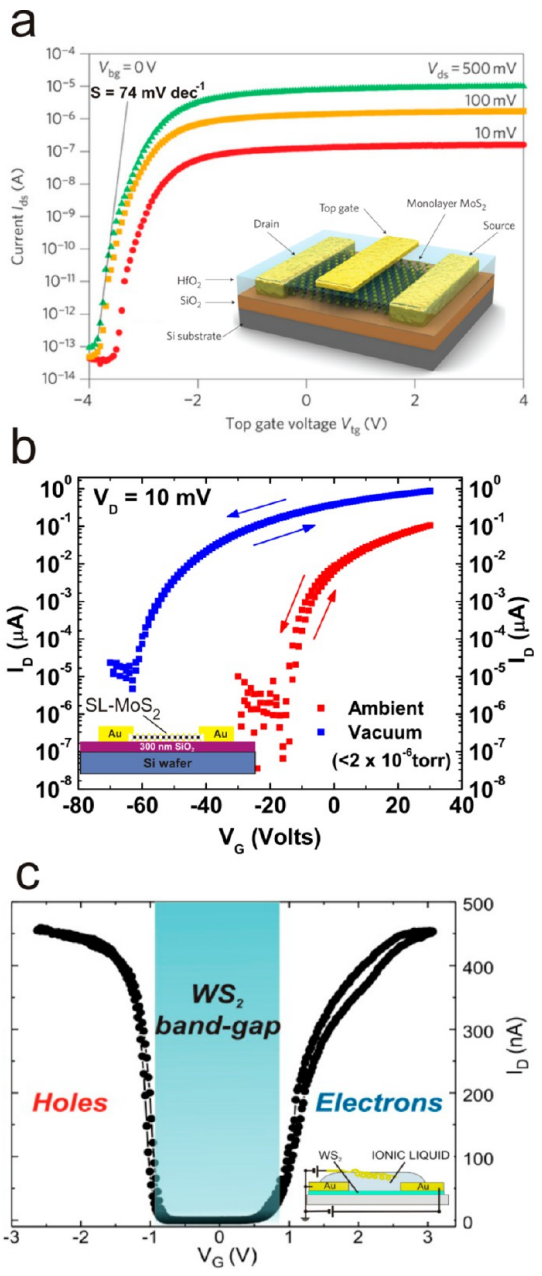

Figure 2. Gate dielectric choices for semiconducting TMDC FETs. (a) Semilog transfer characteristics of a top-gated SL-MoS_2 FET with a 30 nm thick hafnia dielectric. The low subthreshold swing, low operating voltage, and high on/off ratio result from enhanced gate coupling. The inset shows a device schematic. Adapted with permission from ref 16. Copyright 2011 Macmillan Publishers Ltd. (b) Semilog transfer curves of an unencapsulated bottom-gated SL-MoS_2 FET measured under ambient (red) and vacuum (2 × 10^{-6} Torr) (blue), showing that atmospheric adsorbates have deleterious effects on device performance. The inset shows a device schematic. Adapted with permission from ref 82. Copyright 2013 American Institute of Physics. (c) Ambipolar transfer characteristic of an ion-gel-gated few-layer WS_2 FET. The band gap of the sample can be estimated from the width of the off-state. The inset shows the measurement schematic. Adapted from ref 94. Copyright 2012 American Chemical Society.

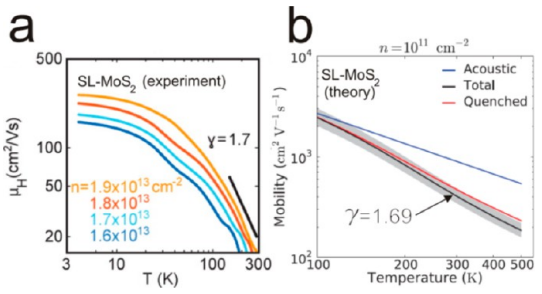

Figure 3. Temperature dependence of carrier mobility. (a) Hall mobility values in single-layer MoS_2 at different carrier densities as a function of temperature. The temperature exponent γ obtained from the experimental data agrees well with the theoretical estimate in (b). Adapted from ref 102. Copyright 2013 American Chemical Society. (b) Calculated carrier mobility as a function of temperature for single-layer MoS_2. The black curve represents the temperature dependence of mobility considering charge scattering by both acoustic and optical phonons. The red curve shows mobility when out-of-plane optical phonons are quenched, while the blue curve considers only acoustic phonons. Adapted with permission from ref 105. Copyright 2012 American Physical Society.

The sensitivity of carrier mobilities to the local dielectric environment has inspired more thorough investigations of their role in charge transport. The first reports of temperature-dependent transport in ultrathin MoS_2 revealed variable range hopping[98] or thermally activated[101] transport as opposed to the band-like transport observed in bulk single crystals.[15] Following improvements in sample quality and device processing, band-like transport was observed in SL-MoS_2 with phonon scattering dominant for $T >$ 100 K and charged impurity scattering dominant for $T <$ 100 K.[80,82,102] Similar behavior has also been reported on few-layer MoS_2[103] and $MoSe_2$.[104] A transition from variable range hopping to band-like transport with increasing carrier density was also observed in SL-MoS_2.[80,102] In this case, the mobility (μ) follows an inverse power law relation with temperature ($\mu \propto T^{-\gamma}$) for $T >$ 100 K, where the exponent γ decreases from 1.4 to 0.7 after encapsulation with HfO_2. In addition, the value of γ also falls from 1.7 in monolayer (Figure 3a) to 1.1 in bilayer unencapsulated devices.[102] In both of these examples, the presence of a top layer quenches/stiffens the homopolar A_{1g} mode to reduce γ as predicted by theory (Figure 3b).[105] However, the experimentally observed reduction in γ is much larger than the predicted value, which suggests that additional scattering mechanisms are active at higher temperatures.[106] Most theoretical work[105−108] has accounted only for intrinsic MoS_2 phonons, leading to the conclusion that longitudinal acoustic phonon scattering is dominant. More recent studies have considered the influence of remote interfacial phonons from the oxide dielectric[109] (akin to graphene[110]), which has led to better agreement with experimental observations.

While it is clear that phonon scattering is important at high temperatures, the disagreement between the theoretically predicted intrinsic mobility and the experimentally measured mobility in the best performing devices warrants further discussion. Theoretical studies have now predicted that the intrinsic mobility at room temperature in SL-MoS_2 is ~300−400 cm^2/Vs at high carrier densities of ~10^{13}/cm^2.[105,107] This value is approximately 5 times greater than the largest experimentally reported values at 300 K,[82] suggesting that room temperature mobilities are further degraded by charged impurities and suboptimal sample quality.[111] While early calculations neglected impurities/defects and thus overestimated mobility values, the qualitative dependence of mobility on carrier density does fall in line with experimental observations. In particular, the mobility has a weak dependence on carrier density at all temperatures except $T <$ 10 K, where the dependence is strong.[108] This temperature dependence can be explained by charged impurity dominated scattering at low temperatures, where a higher carrier density better screens the charges and leads to higher mobility. It should be noted that all of the above studies focused on electronic transport in the low-field limit. Although initial theoretical work on field-dependent mobility[107,109] and high-field transport experiments[112−114] appears promising, a detailed study on the field dependence of mobility in ultrathin chalcogenides is currently absent.

Flicker noise or 1/*f* noise can be a limiting factor for electronic device applications. In particular, the all-surface structure of ultrathin TMDCs makes them sensitive to random perturbations in the environment. In a recent study, the lowest Hooge parameter in high-mobility SL-MoS_2 was found to be 0.005 in vacuum, which is comparable to the noise amplitudes of carbon nanotubes and graphene.[83] However, since the Hooge parameter increases by as much as 3 orders of magnitude in ambient conditions, noise studies confirm the sensitivity of SL-MoS_2 to adsorbates and trapped charges, further suggesting that encapsulation strategies[115] may be effective in reducing the noise amplitude in TMDCs.

The contact resistance from metal electrodes plays an important role in determining the conductance of fully fabricated devices fabricated from reduced dimension materials. In the case of ultrathin MoS_2, commonly used Au contacts show linear current−voltage curves, suggesting ohmic contacts to MoS_2[16,82,98,116] (Figure 4a). This result is counterintuitive since Au has a high work function (5.1 eV) and thus should form a Schottky barrier with n-type MoS_2 (electron affinity ~4.0 eV). However, the width of the resulting Schottky barrier is exceptionally narrow due to the atomically thin TMDC, which enables low resistance tunneling through the barrier.[99] The net result is linear or electrically ohmic transport for ultrathin MoS_2 FETs even with high work function metal contacts.[99] Systematic studies of various metal contacts in ultrathin

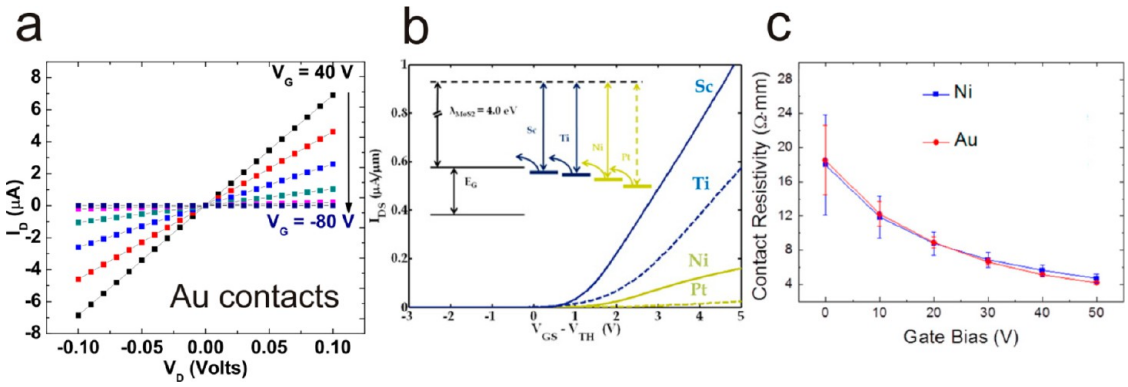

Figure 4. Metal contacts. (a) Linear I_d-V_{ds} output curves in an unencapsulated, bottom-gated single-layer MoS_2 FET with Au contacts. Adapted with permission from ref 82. Copyright 2013 American Institute of Physics. (b) Increase in drain current of a few-layer MoS_2 FET with decreasing work function of the contact metals. Adapted from ref 99. Copyright 2012 American Chemical Society. (c) Gate voltage dependence of the contact resistance in a few-layer MoS_2 FET indicative of a Schottky barrier at the contacts. Adapted from ref 129. Copyright 2012 American Chemical Society.

semiconducting TMDC transistors have also been performed both theoretically and experimentally.[99,117−122] These studies found that low work function metals (*e.g.*, titanium and scandium) form lower resistance contacts than do high work function metals, leading to higher drain currents (Figure 4b).[99] The use of an ultrathin MgO[123] or TiO_2[124] barrier between a ferromagnetic metal and MoS_2 also minimizes Schottky barrier formation. Similarly, contact doping with nitrogen dioxide (NO_2),[125] elemental potassium,[126] and polyethylenimine (PEI)[127] has also been achieved in semiconducting TMDC FETs.

Nevertheless, even with an optimal contacting scheme, the contact resistance ultimately dominates charge transport with reduced channel dimensions.[128] This effect manifests itself as reductions in drain current and mobility at channel lengths below 500 nm,[128,129] although quantum transport simulations predict excellent length scaling down to 10−15 nm.[130−132] The contact resistance of Au and Ni was also found to be a strong function of the applied gate bias,[102,129] which suggests the presence of gate-tunable Schottky barriers (Figure 4c). It is therefore likely that field-effect mobilities reported in two-probe devices are in general underestimated due to these contact effects. The reported values of contact resistance with Au[102,129,133] also vary widely, suggesting that changes in the surface cleanliness, sample quality, annealing, vacuum level, and method of evaporation can also have significant effects on the metal−semiconductor contact.

Overall, this section highlights several aspects of ultrathin semiconducting TMDC FETs that require deeper understanding and optimization to compete with conventional materials (*e.g.*, Si and GaAs) in high-performance transistors. However, in the near term, semiconducting TMDCs show promise in flexible, stretchable, and/or transparent electronics. Figure 5 shows a comparison of field-effect mobilities and on/off ratios for all candidate semiconductors that

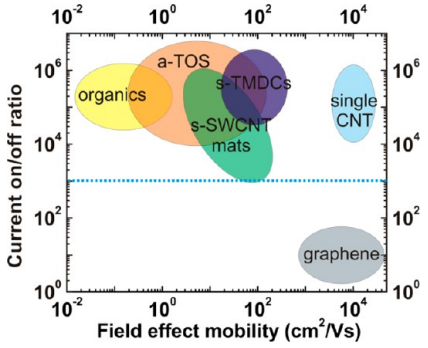

Figure 5. Comparison of field-effect mobility and on/off ratios of semiconductors for unconventional electronics. High on/off ratios (>10^3) are essential for digital electronics applications while maintaining the highest mobility possible. Semiconducting TMDCs (s-TMDCs) lie on a favorable position on this plot compared to other semiconductors that are currently under consideration for large-area flexible electronics.

are being evaluated for these unconventional macroelectronic applications. As is evident from this figure, despite a significantly shorter history, semiconducting TMDCs have comparable mobilities and on/off ratios to organics,[26,27,30] amorphous oxide semiconductors,[134,135] and semiconducting carbon nanotube networks.[136,137] The availability of flexible contacts and dielectrics (*e.g.*, graphene, h-BN, and ion gels) has also enabled the fabrication of flexible, ultrathin electronic devices entirely from layered two-dimensional materials.[89] These initial studies demonstrate that ultrathin semiconducting TMDC FETs on flexible substrates are robust to mechanical bending with the important device parameters (*e.g.*, mobility, on/off ratio, and on-current) remaining within a desirable range.[138,139] Flexible FETs from chemical vapor deposition (CVD)-grown MoS_2 have also been demonstrated using ion gel dielectrics, which suggests large-area scalability of this device class.[140]

Inverters and Logic Gates. Since semiconducting TMDCs show promise as high performance FETs,

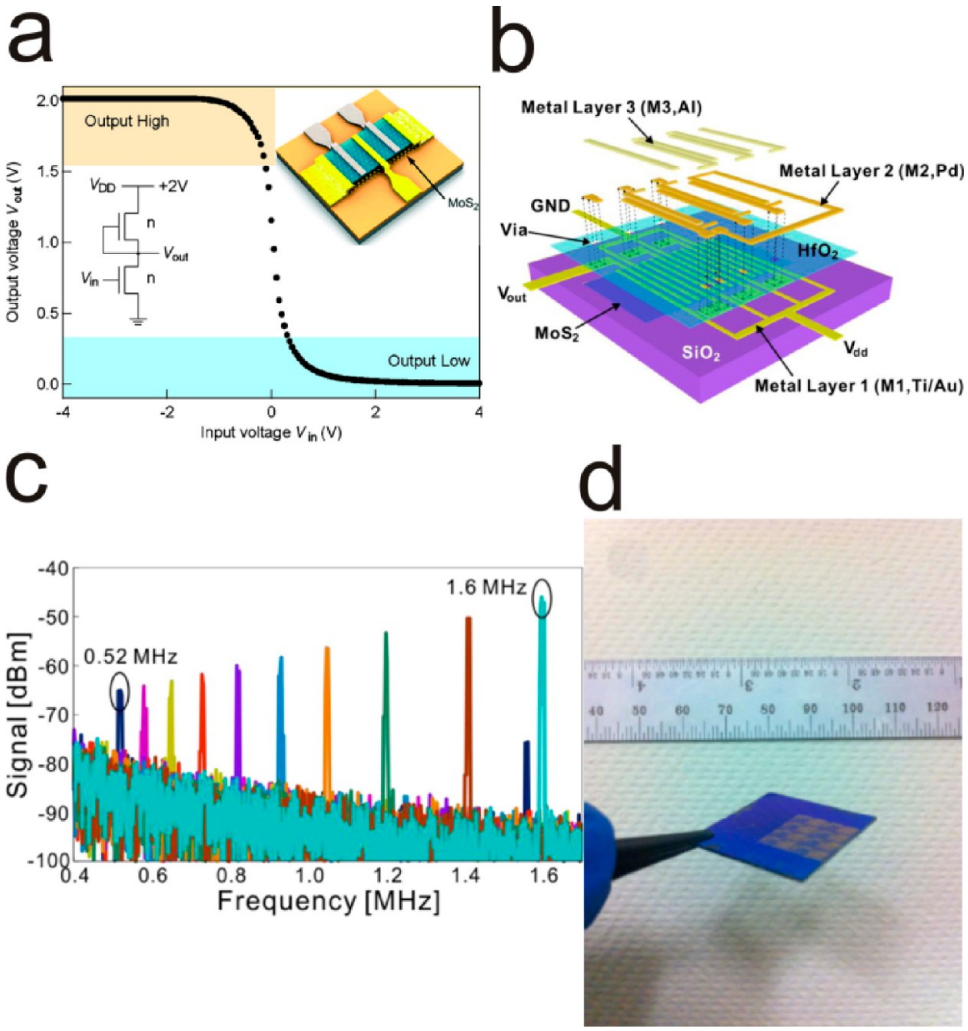

Figure 6. Integrated circuits from ultrathin semiconducting TMDCs. (a) Output voltage as a function of input voltage of an inverter based on two single-layer MoS_2 FETs. The inset shows the circuit diagram (left) and device schematic (right). Adapted from ref 141. Copyright 2011 American Chemical Society. (b) Schematic illustration of a ring oscillator circuit fabricated on ultrathin MoS_2. (c) Power spectrum of the ring oscillator output signal as the supply voltage (V_{dd}) is increased from left to right. Adapted from ref 142. Copyright 2012 American Chemical Society. (d) Demonstration of electronic devices on chemical vapor deposition grown single-layer MoS_2 over large areas. Adapted with permission from ref 143. Copyright 2012 Institute of Electrical and Electronics Engineers.

researchers have begun integrating them into more complex, functional digital circuitry including inverters and logic gates. An inverter typically consists of two FETs in series and is designed to convert logical 0 (low input voltage) to logical 1 (high output voltage) and *vice versa*. The common electrode between the two FETs serves as the output, while the gates of the FETs serve as the input (Figure 6a inset). An important metric for an inverter is the voltage gain, which is characterized by the negative derivative of the output plot (Figure 6a).[141] Single-layer MoS_2 inverters were first reported in 2011.[141] Thereafter, several reports of inverters based on a variety of semiconducting TMDCs have been published with gains varying between 2 and 16.[21,142−144] A gain greater than unity is required in circuits consisting of cascaded inverters such as ring oscillators. In particular, a ring oscillator possesses an odd number of inverters in series to produce high-frequency clock signals (Figure 6b).[142] Ring oscillators have been successfully demonstrated with MoS_2, leading to operating frequencies up to 1.6 MHz with stage delays of ~60 ns (Figure 6c).[142] Although this performance is inferior to ring oscillators based on conventional silicon, graphene,[145] or carbon nanotubes,[146] it is superior to current generation organics and amorphous oxide semiconductors,[147−149] which strengthens the case for semiconducting TMDCs in unconventional electronic applications. Similarly, NAND gates and static random access memory (SRAM) cells containing 3 and 4 FETs, respectively, have been demonstrated with ultrathin MoS_2.[142,143]

A majority of the above reports are based on mechanically exfoliated TMDC flakes. However, practical manufacturing will require the production of large-area materials *via* scalable approaches. Toward that end, several groups have demonstrated the

synthesis of atomic layers and multilayers of TMDCs using CVD techniques,[150−155] thus enabling fabrication of large-area electronics from atomically thin TMDC semiconductors (Figure 6d).[143] Note, however, that the carrier mobility in the CVD-grown materials is about an order of magnitude lower than in mechanically exfoliated flakes, and thus significant improvements in growth techniques will be required.[152,153,156] Despite substantial progress in a short time span, all TMDC-based devices and circuits are unipolar in character thus far, which leads to high power consumption in inverters and logic gates. In contrast, complementary metal-oxide−semiconductor (CMOS) circuits enable low static power consumption, logic gate cascading, and highly integrated circuitry. Therefore, CMOS-based circuits using semiconducting TMDCs represent a key future goal for this field. In addition to controllable complementary doping schemes (*i.e.*, both n-type and p-type), methods for tailoring threshold voltage for complementary enhancement-mode FETs will be required.[157] Controlling doping and threshold voltages in atomically thin semiconductor devices has presented a major challenge since even a fractional percentage of substitutional doping can significantly degrade carrier mobility or alter the band structure. On the other hand, charge transfer doping by noncovalent functionalization/adsorption of dopant species has been effective in preserving the material quality, but this approach presents issues of long-term stability. While the above challenges have plagued the field of carbon nanomaterials, naturally occurring chalcogen vacancies in TMDCs generate free carriers, and thus, controlled substitution/vacancy formation (without altering the band structure) may present a viable path forward in addition to stable, noncovalent charge transfer doping schemes. The reduced dimensionality of the conduction channel presents a similar challenge with threshold voltage control since the addition of more charges degrades carrier mobility. A combined approach involving doping as well as work function control of the gate electrode may present a viable solution for engineering threshold voltages in semiconducting TMDC field-effect devices.

Junctions and Heterostructures. In addition to devices and circuits based on individual semiconducting TMDC materials, these materials present opportunities for unique device geometries based on junctions and heterostructures.[158,159] Such heterojunction devices have been widely developed for crystalline III−V semiconductors for high-frequency applications. These III−V semiconductor heterostructures have been historically grown by epitaxial crystal growth methods (*e.g.*, molecular beam epitaxy), which limits the range of possible heterojunctions to those materials that possess closely matched lattice parameters. On the other hand, the relatively weak van der Waals bonding between TMDCs relaxes this constraint and thus suggests a broader range of possible junctions and heterostructures.[10]

The use of ultrathin materials in vertical heterostructures also allows partial penetration of electric fields through the entire stack, thereby enabling gate tunability of the heterointerface.[160−162] The first demonstration along these lines was a tunneling field-effect transistor (TFET) that consists of a graphene/TMDC/graphene sandwich (Figure 7a),[160,163] where the TMDC acts as a tunnel barrier (Figure 7b inset). In this structure, the tunneling probability can be controlled by tuning the Fermi level of the graphene by a gate voltage, thereby modulating the tunneling current between the two graphene layers by up to 6 orders of magnitude (Figure 7b).[160] This high current on/off ratio was confirmed independently by theory.[164] Heterostructure TFETs were subsequently fabricated on flexible substrates, where they exhibited high resilience to bending.[160] Likewise, a vertical heterojunction between a semimetal (graphene) and a semiconductor (MoS_2) creates a two-dimensional Schottky barrier at the interface that can be tuned by a gate voltage.[161] This concept was extended further to create a functional inverter by vertical stacking n-type and p-type layers separated by graphene layers as interconnects.[165]

The charge transport in graphene/TMDC/graphene structures and their variants occurs *via* a combination of tunneling (through the barrier) and thermionic (over the barrier) modes. The dominant mechanism depends on the thickness of the TMDC semiconductor, gate voltage, and temperature.[160,163,165] At lower TMDC thicknesses (1−5 nm), tunneling through the barrier dominates and thus a thicker TMDC (>5 nm) leads to lower currents in the off-state (negative gate voltages) and high on/off ratios.[160] For positive gate voltages and higher temperatures, the thermionic current over the barrier dominates charge transport. However, increased screening in thicker TMDCs leads to poor gate modulation of the top layer (further from the gate electrode) barrier, thereby limiting on-current density.[165] This trade-off between on/off ratio and on-current density can be partially circumvented using a metal contact at one end (instead of graphene) to pin the TMDC Fermi level.[165]

The absence of dangling bonds on TMDC basal planes presents additional opportunities to combine them with amorphous materials such as oxides, polymers, and organic small molecules. For example, ultrathin memory devices have been demonstrated using such combinations.[166−168] The earliest report of a semiconducting TMDC memory device involved using a ferroelectric polymer as the top dielectric and charge-trapping layer.[168] Later demonstrations used graphene as both the contact and floating gate with MoS_2 as the channel and ALD-derived alumina as the tunnel barrier.[166] An alternative geometry employed h-BN as a tunnel barrier sandwiched between a MoS_2 FET and a

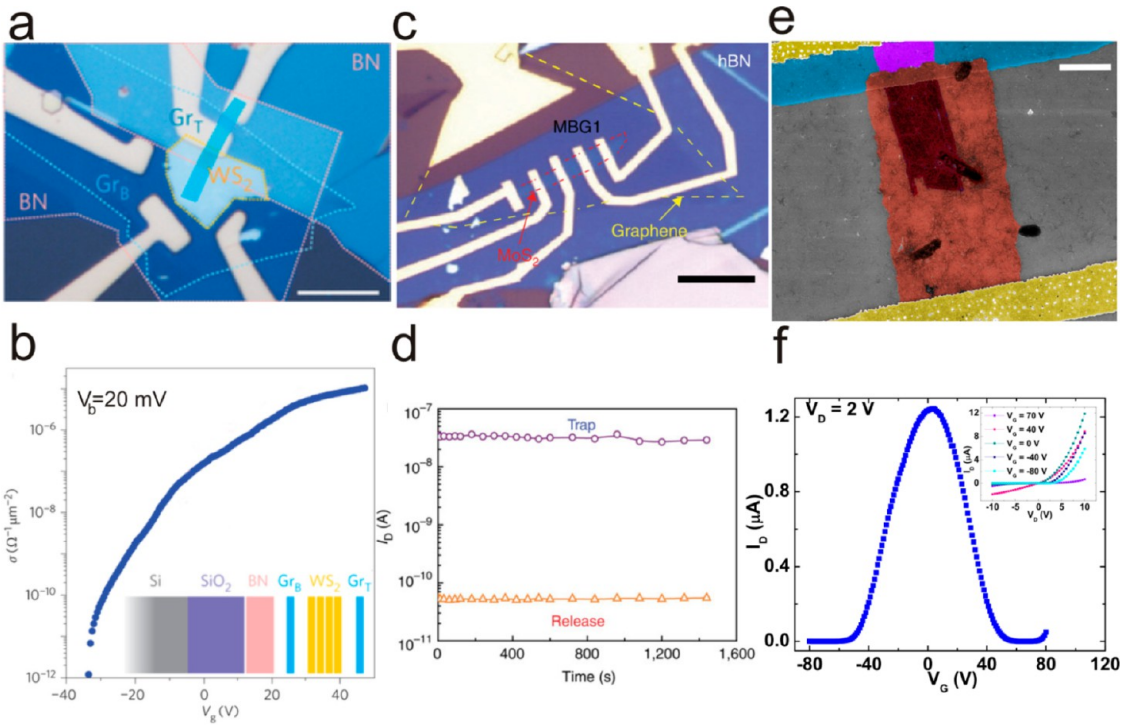

Figure 7. van der Waals heterostructure devices. (a) Optical micrograph of a tunneling field-effect transistor (TFET) composed of a graphene/WS_2/graphene sandwich encapsulated between h-BN layers on the top and bottom. Gr_b and Gr_t stand for bottom and top graphene, respectively. (b) Semilog transfer curve of the same device showing on/off ratios >10^6. The inset shows a schematic diagram of the device cross section. Adapted with permission from ref 160. Copyright 2013 Macmillan Publishers Ltd. (c) Optical micrograph of a MoS_2/h-BN/graphene memory cell with the layer boundaries appropriately colored. (d) Temporal current stability through the MoS_2 channel of the same device after applying the write (trap) and erase (release) pulses. Adapted with permission from ref 167. Copyright 2013 Macmillan Publishers Ltd. (e) False-colored scanning electron micrograph of a s-SWCNT/SL-MoS_2 p-n heterojunction. The dark red region is the MoS_2 flake, which is colored pink as it goes under the atomic layer deposition grown alumina (blue). The pink rectangle is a patterned film of randomly oriented semiconducting SWCNTs. (f) Anti-ambipolar transfer curve of the same device with two off-states and a current peak between them. The inset shows the gate dependence of the output curves of the diode ranging from an insulating to a highly rectifying state. Adapted with permission from ref 173. Copyright 2013 National Academy of Sciences, U.S.A.

graphene floating gate (Figure 7c,d).[167] These memory cells outperformed organic semiconductor-based memories in terms of retention time and endurance.[167] Bulk heterojunctions of chemically exfoliated MoS_2 and graphene oxide (GO) have also been used to fabricate memory devices, albeit with much poorer performance compared to the planar heterostructures discussed above.[169,170]

While TFETs, memory cells, and inverters have been realized using semiconducting TMDCs in layered heterostructures, the p-n junction is relatively unexplored. Note that p-n junctions based on bulk semiconducting TMDCs have been known for decades,[171,172] but the lack of controlled doping strategies and the limited availability of ultrathin p-type semiconducting TMDCs have thus far prevented the realization of purely two-dimensional p-n heterojunctions. However, a p-n heterojunction can be fabricated by vertical stacking an n-type single-layer TMDC (*e.g.*, MoS_2, WS_2, or $MoSe_2$) with another p-type semiconductor such as semiconducting single-walled carbon nanotubes (s-SWCNTs)[173] or other conventional semiconductors.[174] For example, a gate-tunable p-n heterojunction diode has been achieved by vertical stacking n-type SL-MoS_2 and p-type semiconducting SWCNT thin films (Figure 7e).[173] The resulting p-n heterojunction diode not only shows gate-tunable rectification (Figure 7f inset) but also exhibits a unique "*anti-ambipolar*" transfer curve with two off-states and a conductance maximum in between them (Figure 7f).[173] While charge transport mechanisms in all 2D materials such as graphene/TMDC heterostructures have been investigated to some extent as discussed above, the mechanisms in heterojunctions of mixed dimensionality components are not well-understood. Further work will thus be required to understand issues such as band alignment, depletion regions, excess carrier separation, and interfacial charge transport mechanisms in these atomically thin p-n heterojunctions.

Gate tunability is not limited to the vertically stacked heterostructure geometry. In fact, each side of a lateral heterojunction can be independently tuned by individually addressable gates. As discussed above, the ultrathin nature of semiconducting TMDCs enables the subthreshold swing to be less than 80 mV/dec in top-gated SL-MoS_2 FETs at room temperature, thus

making TMDCs attractive candidates for interband tunneling FETs. Initial theoretical work has proposed potential device geometries and indicated that a lower band gap semiconducting TMDC would be the most suitable candidate.[175,176] Some efforts to create lateral p-n junctions from MoS_2 have been made, notably by ion gel gating an ambipolar device such that $V_{ds} > V_{gs}$[177] (V_{ds} and V_{gs} represent voltages applied between drain-source and gate-source contacts, respectively) and selective p-type doping of an MoS_2 flake by exposure to various plasmas.[178,179] In-plane p-n heterojunctions from two disparate semiconducting TMDCs are also an enticing possibility considering that ternary two-dimensional alloys of $Mo_xW_{1-x}S_2$ and $MoS_{2(1-x)}Se_{2x}$ have already been synthesized.[180−183] It is, however, expected that precise control over growth and lattice matching will present issues such as chalcogen intermixing and control over dopant density in selective areas, and thus in-plane engineering of two-dimensional heterostructures and p-n junctions may be more constrained than their vertical heterojunction counterparts. Since the band structures of semiconducting TMDCs undergo dramatic changes with thicknesses in the 1−6 layer limit,[44] thickness-dependent lateral junctions are another possibility. For example, one such lateral junction between monolayer and bilayer graphene exhibited a photothermoelectric response.[184] Furthermore, some approaches to create thickness-dependent lateral TMDC junctions are already in place,[185−187] although no working devices have yet been demonstrated.

Optoelectronics. With direct band gaps in the visible portion of the electromagnetic spectrum, large exciton binding energies, and strong photoluminescence, monolayer semiconducting TMDCs are promising for optoelectronic applications. Several classes of optoelectronic devices have been demonstrated from ultrathin semiconducting TMDCs including photodetectors, photovoltaics, and light-emitting devices. This section will review these applications in detail.

Photodetectors. When photons of energy greater than the band gap are incident on a semiconductor, they create bound electron−hole pairs (excitons) or free carriers depending on the exciton binding energy in the semiconductor. Bound excitons separated by an applied or built-in electric field generate a photocurrent. Two major categories of semiconductor-based photodetectors exist, namely, phototransistors and photodiodes.

Initial studies on ultrathin MoS_2-based phototransistors measured photocurrent under global illumination[188,189] with photons possessing energies greater than the 1.9 eV band gap (Figure 8a).[189] Phototransistors have also been recently extended to chemical vapor deposition grown few-layer WS_2.[190] Wavelength-dependent studies later suggested that the photocurrent roughly follows the absorption spectrum, which led to speculation of interband absorption and carrier separation as the dominant mechanism of photocurrent generation.[188,191] In this context, scanning photocurrent microscopy has emerged as a powerful tool to elucidate the underlying photocurrent generation mechanisms in nanoscale devices.[192,193] An initial report of scanning photocurrent measurements on unbiased SL-MoS_2 devices claimed that the photothermoelectric effect is the dominant mechanism for photocurrent generated near the contacts.[116] Subsequent studies on the bias dependence of spatially resolved photocurrents in MoS_2 FETs suggested interband excitation as the dominant photocurrent mechanism under bias (Figure 8b,c), although the relative contributions from the two mechanisms at zero bias may vary between devices.[194] At large drain biases (*i.e.*, saturation regime), the electric field is large enough to separate photoexcited electron−hole pairs across the channel, thereby leading to a larger net photocurrent in the channel (Figure 8d).[195] Most phototransistors operating under bias achieve larger than unity responsivity (often $R > 10^3$ A/W) *via* internal amplification of the photocurrent. For example, the graphene-MoS_2 vertical heterostructure channel led to phototransistors with $R > 10^7$ A/W (Figure 8d),[196,197] similar in concept to quantum dot sensitized graphene photodetectors.[198] Despite such high responsivities, phototransistors suffer from relatively long response times compared to photodiodes.[199]

A photodetector can have short response times if the photogenerated carriers are separated and collected within a short distance by a built-in electric field. For ultrafast photodetectors, built-in fields are achieved *via* a variety of junctions including semiconductor−metal Schottky junctions, homojunctions between differently doped regions in a semiconductor, and heterojunctions between two different semiconductors. Although Schottky junctions are the main source of the low bias photoresponse in most reports of MoS_2 phototransistors, the concept of a metal−semiconductor−metal (M−S−M) junction has been systematically exploited only recently.[200,201] This approach enables a faster response time as compared to conventional FETs primarily due to the reduced channel length between the two M−S junctions. In particular, intrinsic speed limits of a M−S−M photodetector can be achieved if the channel length is reduced to less than twice the depletion width. Such photodetectors comprising vertical stacks of graphene/TMDC/graphene have been demonstrated with response speeds down to 50 μs.[202] Nevertheless, a p-n heterojunction photodiode presents opportunities for even faster photodetection. Heterojunctions of p-type Si (crystalline[203] and amorphous[204]) with n-type MoS_2 have now been realized. In addition, the aforementioned gate-tunable p-n heterojunction diode based on p-type semiconducting SWCNTs and n-type

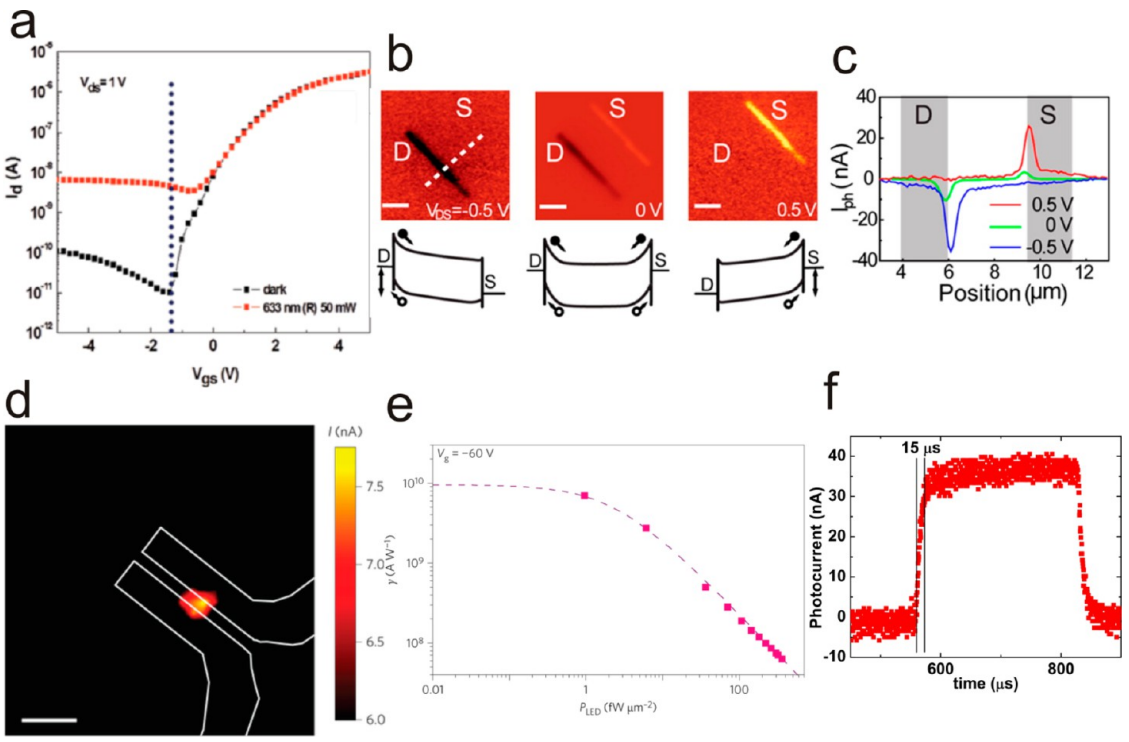

Figure 8. Photodetectors from s-TMDCs. (a) Semilog transfer curves of a few-layer MoS_2 photo-FET in dark (black) and under illumination (red). Photocurrent is seen in depletion mode. The inset shows the device schematic adapted with permission from ref 189. Copyright 2012 Wiley-VCH. (b) Spatial photocurrent maps of a few-layer MoS_2 FET under varying V_{ds}. The photocurrent magnitude at the source (drain) increases (decreases) under forward bias and *vice versa* for reverse bias with corresponding schematic band diagrams below. (c) Line profiles of the photocurrents in (b) along the dashed white line. Adapted from ref 194. Copyright 2013 American Chemical Society. (d) Spatial photocurrent map of a single-layer MoS_2 FET under bias. Drift-field-induced photocurrent generation from the entire channel can be seen. The inset shows the schematic of the device with laser beam. Adapted with permission from ref 195. Copyright 2013 Macmillan Publishers Ltd. (e) Photoresponsivity *versus* incident power of a graphene/MoS_2 bilayer photo-FET. The inset shows the device schematic. Adapted with permission from ref 196. Copyright 2013 Macmillan Publishers Ltd. (f) Fast photoresponse from a s-SWCNT/SL-MoS_2 p-n heterojunction diode. An instrument-limited rise time of 15 μs can be seen. Adapted with permission from ref 173. Copyright 2013 National Academy of Sciences, U.S.A.

SL-MoS_2 exhibits a fast photoresponse (rise time <15 μs, limited by instrumentation) (Figure 8e) with peak responsivity of ~0.1 A/W.[173] van der Waals p-n heterojunctions between semiconducting TMDCs and other direct band gap materials are expected to show similar results.

Solar Cells and Light-Emitting Devices. The photovoltaic cell is one of the most widespread applications of a p-n junction. As per the Shockley–Quessier limit, a high-mobility semiconductor with a direct band gap near 1.3 eV is desired for high-efficiency single junction photovoltaics. Single-layer semiconducting TMDCs are well-positioned here in terms of both direct band gap and mobility values (Figure 9), making them promising candidates for photovoltaic applications. Among several recent theoretical studies, one calculation on a Schottky junction solar cell consisting of a graphene–MoS_2 stack suggests a maximum power conversion efficiency (PCE) of ~1% while that of a type-II heterojunction between WS_2/MoS_2 is 1.5%.[205] Experimentally, an asymmetric M–S–M Schottky junction on a few-layer MoS_2 flake resulted in working photovoltaic devices with ~1% PCE,[206] while split-gated p-n

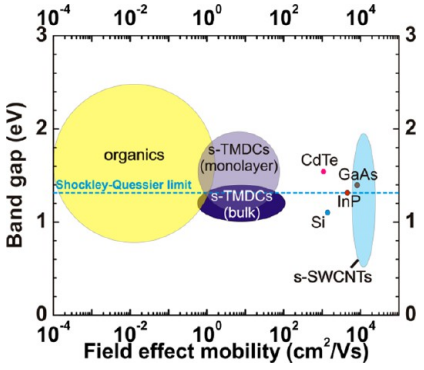

Figure 9. Band gap *versus* field-effect mobility for important semiconductors used in current generation photovoltaic technologies. A band gap near the Shockley–Quessier limit (~1.3 eV) and high mobilities are expected to lead to high-efficiency photovoltaic devices. Semiconducting TMDCs are favorably placed in comparison to organic semiconductors for flexible photovoltaic cells.

junctions on monolayer WSe_2 achieved a PCE of 0.5%.[207] Recently, vertically stacked graphene/TMDC/graphene structures have also shown promise with external quantum efficiency values as high as 55% at a

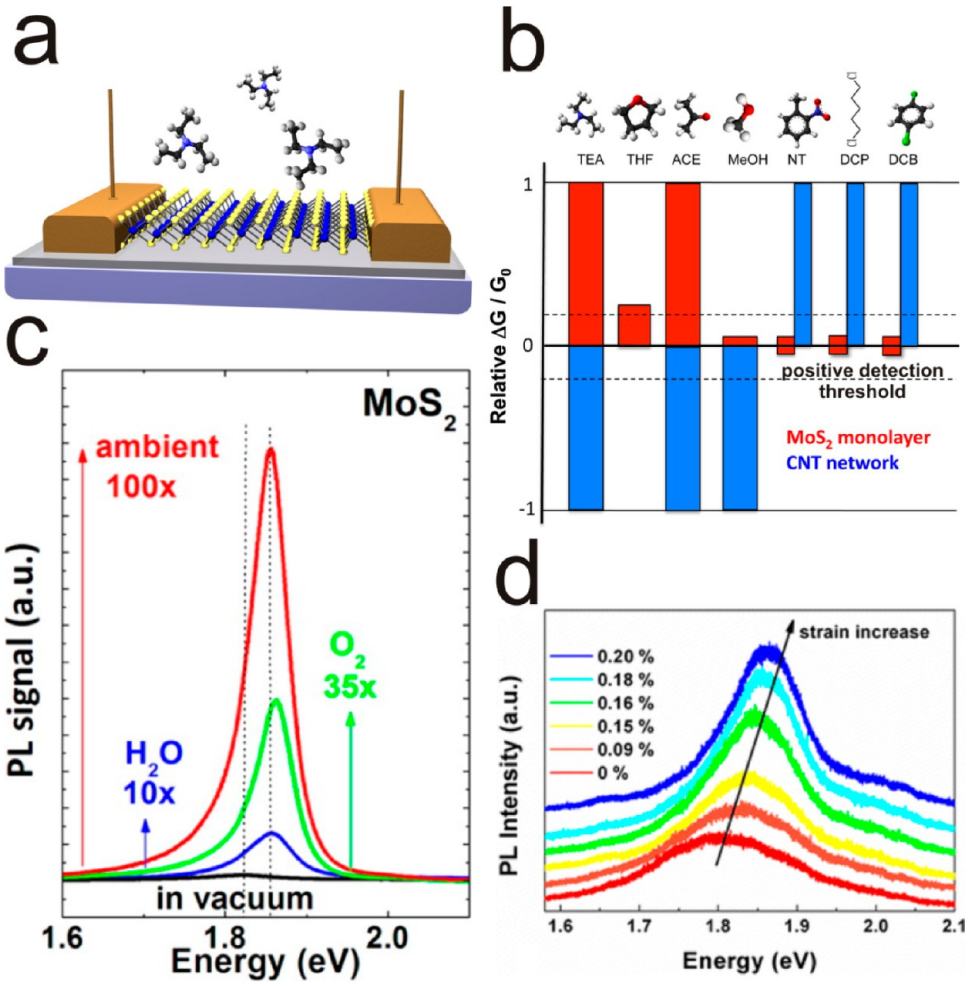

Figure 10. Sensors from semiconducting TMDCs. (a) Schematic of a single-layer MoS_2 FET sensing small organic analytes. (b) Sensitivity of a single-layer MoS_2 FET (red) compared with a random network SWCNT FET. The higher selectivity of single-layer MoS_2 over SWCNTs can be seen. Adapted from ref 217. Copyright 2013 American Chemical Society. (c) Photoluminescence (PL) efficiency of single-layer MoS_2 in the presence of various gaseous adsorbates. Adapted from ref 222. Copyright 2013 American Chemical Society. (d) PL spectra from a single-layer MoS_2 FET under varying amount of strain. Adapted from ref 223. Copyright 2011 American Chemical Society.

single wavelength.[202] Although the above results for ultrathin solar cells based on semiconducting TMDCs are encouraging, thickness-limited absorption poses a challenge for high efficiency. To overcome this issue, light-trapping techniques such as plasmon-enhanced absorption,[208−210] strain engineering,[211] and/or vertical stacks of atomically thin cells are being pursued.

The light-emitting diode (LED) is another ubiquitous application of the p-n junction. As direct gap materials, monolayer semiconducting TMDCs are a promising option for ultrathin, efficient, and flexible LEDs. However, the lack of controlled doping strategies has thus far hindered LEDs fabricated from purely monolayer TMDCs. Nevertheless, Schottky junction based light-emitting devices have been realized albeit with low quantum efficiencies ($\sim 10^{-5}$).[212] Based on the heterojunction photodetection mechanism mentioned above, excitonic electroluminescence has also been observed from SL-MoS_2 and crystalline p-type Si heterojunctions.[203] Homojunctions formed by electrostatic doping of nearly intrinsic monolayer WSe_2 have also resulted in atomically thin LEDs with maximum efficiencies of ~0.2%.[207,213,214] With commercial organic LEDs approaching 20% emission efficiencies, improvements in doping, surface engineering, encapsulation, and device design are needed for semiconducting TMDCs to be competitive light emitters.

Sensors. Electronic sensors exploit changes in the electrical properties of constituent materials upon interaction with an analyte. When a bulk material in a FET channel interacts with an analyte, its resistance or the device capacitance typically undergoes relatively small changes since the interaction is limited to the surface. However, in atomically thin nanomaterials, the surface-to-volume ratio is close to unity and thus the electrical properties are significantly perturbed by even submonolayer analyte adsorption (Figure 3b). This strategy has been heavily exploited in carbon nanomaterials[3] and should also apply to ultrathin semiconducting TMDCs.

Initial studies on TMDC-based gas sensing employed MoS_2 FETs for the detection of nitrogen monoxide (NO). The resistance of single-layer and few-layer MoS_2 FETs was found to be sensitive to the presence of NO down to 0.8 ppm in a N_2 environment.[215] A subsequent study focused on elucidating the effect of gate voltage (*i.e.*, carrier concentration), layer thickness, and analyte type (reducing or oxidizing) on the sensing properties. It was found that multilayer MoS_2 (5 layers) was the most sensitive to all of the analytes under consideration (*i.e.*, NO_2, NH_3, and H_2O). In addition, a positive gate bias (*i.e.*, accumulation) has the opposite effect on the sensitivity of reducing (NH_3) *versus* oxidizing (NO_2) analytes.[216] The authors concluded that charge transfer to the MoS_2 channel underlies the sensing mechanism, although some ambiguity remains regarding the effect of contact doping as observed in the case of WSe_2 FETs.[125] Another detailed study using small organic molecule analytes observed that the sensitivity of the SL-MoS_2 FET channel (Figure 10a) was highest for the most reducing and polar analytes while the channel was insensitive to oxidizing analytes. Such selectivity was not observed for the comparative case of carbon nanotube network sensors (Figure 10b).[217] While all of the above studies were performed on mechanically exfoliated flakes, attempts at scaling up MoS_2 chemical sensors have been recently made using chemical vapor deposition films[218] and solution-phase exfoliated flakes.[219−221]

In addition to sensing based on changes in resistance, monolayer semiconducting TMDCs also provide an alternative avenue for sensing based on light emission. In particular, the physisorption and resulting charge transfer upon analyte binding leads to changes in the PL/EL emission efficiencies depending on the polarity of the semiconductor. This strategy has been demonstrated using electron-withdrawing analytes (*e.g.*, O_2 and H_2O), which enhance the PL efficiencies of n-type MoS_2 and WS_2 (Figure 10c) while reducing PL efficiencies for p-type WSe_2.[222] The strain-dependent shift in band structure and exciton binding energies of monolayer semiconducting TMDCs have also led to attempts at exploiting this phenomenon for strain sensing (Figure 10d).[223]

Although the field of semiconducting TMDC-based electronic devices has evolved rapidly, studies on sensor development have been relatively limited. Specifically, the issues of selectivity and reset-ability require significantly more attention. Since the performance degradation of TMDC devices due to adsorbate interaction is reversible by subjecting the devices to vacuum conditions, the reset-ability of TMDC-based sensors is likely to be superior to organic semiconductors where this degradation is irreversible. Following previous work on carbon nanomaterials,[3] chemical selectivity can likely be achieved through chemical functionalization methods. Of particular interest will be functionalization strategies that are chemically robust and yet do not significantly perturb the electronic properties of the underlying TMDCs.

CONCLUSIONS AND OUTLOOK

Significant progress has been made in many application areas of semiconducting TMDCs. The bulk of this effort has focused on FETs, where the underlying charge transport and scattering mechanisms have been identified and the effects of dielectrics, environment, and contacts have been delineated. This fundamental knowledge has begun to translate into rudimentary functional electronic circuits, although integration issues such as complementary doping and threshold voltage control require more effort. Similarly, access to high-quality, large-area substrates is emerging with the advent of chemical vapor deposition grown material, although improvements are needed for high-performance circuit applications. For optoelectronics, methods for enhancing light absorption and improving fluorescence and electroluminescence quantum yields in ultrathin materials will be needed if they are to be competitive with conventional bulk semiconductors. Finally, for sensing applications, chemical functionalization methods are desired that impart high chemical selectivity and robustness without disrupting the superlative electronic properties of the TMDC semiconductor.

With regard to the commercialization potential for semiconducting TMDCs, it appears that unconventional formats that require flexibility, stretchability, and/or transparency are most promising. Since even a monolayer (thickness <1 nm) semiconducting TMDC can give a comparable electrical performance to a 10 nm thick organic or amorphous oxide semiconductor, ultrathin TMDCs are particularly well-suited for transparent and flexible electronics. However, with high temperature (>400 °C) chemical vapor deposition as the only known method to obtain electronic grade TMDCs over large areas, direct growth or transfer onto flexible/transparent plastic substrates will pose challenges. Similarly, solution-based methods for preparing and depositing TMDC materials require substantial improvement, especially for high-performance electronic and optoelectronic applications.

While many applications of semiconducting TMDCs are virtually identical to other electronic materials, the atomically thin nature of TMDCs presents unique opportunities. In particular, the gate tunability of heterostructure devices enables fundamentally different charge transport phenomena including the anti-ambipolarity that has been observed in SWCNT/SL-MoS_2 p-n heterojunctions. In such heterostructure devices, the spectral photoresponse can also be tuned with an external gate bias, enabling dynamic tailoring of device characteristics. Since this gate tunability does not exist in bulk semiconductors, devices that exploit it

are unlikely to face competition from conventional materials and thus present unimpeded access to new markets. By focusing directly on such unique opportunities, the technological impact of semiconducting TMDCs can likely be maximized.

Conflict of Interest: The authors declare no competing financial interest.

Acknowledgment. This work was supported by the Materials Research Science and Engineering Center (MRSEC) of Northwestern University (National Science Foundation Grant DMR-1121262) and the Office of Naval Research Multidisciplinary University Research Initiative Program (Grant N00014-11-1-0690).

REFERENCES AND NOTES

1. Novoselov, K. S.; Falko, V. I.; Colombo, L.; Gellert, P. R.; Schwab, M. G.; Kim, K. A Roadmap for Graphene. *Nature* **2012**, *490*, 192–200.
2. Schwierz, F. Graphene Transistors. *Nat. Nanotechnol.* **2010**, *5*, 487–496.
3. Jariwala, D.; Sangwan, V. K.; Lauhon, L. J.; Marks, T. J.; Hersam, M. C. Carbon Nanomaterials for Electronics, Optoelectronics, Photovoltaics, and Sensing. *Chem. Soc. Rev.* **2013**, *42*, 2824–2860.
4. Jariwala, D.; Srivastava, A.; Ajayan, P. M. Graphene Synthesis and Band Gap Opening. *J. Nanosci. Nanotechnol.* **2011**, *11*, 6621–6641.
5. Neto, A. C.; Guinea, F.; Peres, N.; Novoselov, K. S.; Geim, A. K. The Electronic Properties of Graphene. *Rev. Mod. Phys.* **2009**, *81*, 109–162.
6. Nicolosi, V.; Chhowalla, M.; Kanatzidis, M. G.; Strano, M. S.; Coleman, J. N. Liquid Exfoliation of Layered Materials. *Science* **2013**, *340*, 1420.
7. Wang, Q. H.; Kalantar-Zadeh, K.; Kis, A.; Coleman, J. N.; Strano, M. S. Electronics and Optoelectronics of Two-Dimensional Transition Metal Dichalcogenides. *Nat. Nanotechnol.* **2012**, *7*, 699–712.
8. Chhowalla, M.; Shin, H. S.; Eda, G.; Li, L.-J.; Loh, K. P.; Zhang, H. The Chemistry of Two-Dimensional Layered Transition Metal Dichalcogenide Nanosheets. *Nat. Chem.* **2013**, *5*, 263–275.
9. Butler, S. Z.; Hollen, S. M.; Cao, L.; Cui, Y.; Gupta, J. A.; Gutiérrez, H. R.; Heinz, T. F.; Hong, S. S.; Huang, J.; Ismach, A. F.; *et al.* Progress, Challenges, and Opportunities in Two-Dimensional Materials Beyond Graphene. *ACS Nano* **2013**, *7*, 2898–2926.
10. Grigorieva, I. V.; Geim, A. K. van der Waals Heterostructures. *Nature* **2013**, *499*, 419–425.
11. Huang, X.; Zeng, Z.; Zhang, H. Metal Dichalcogenide Nanosheets: Preparation, Properties and Applications. *Chem. Soc. Rev.* **2013**, *42*, 1934–1946.
12. Wilson, J. A.; Yoffe, A. D. The Transition Metal Dichalcogenides Discussion and Interpretation of the Observed Optical, Electrical and Structural Properties. *Adv. Phys.* **1969**, *18*, 193–335.
13. Shishidou, T.; Freeman, A. J.; Asahi, R. Effect of GGA on the Half-Metallicity of the Itinerant Ferromagnet CoS_2. *Phys. Rev. B* **2001**, *64*, 180401.
14. Fivaz, R.; Mooser, E. Electron–Phonon Interaction in Semiconducting Layer Structures. *Phys. Rev.* **1964**, *136*, A833–A836.
15. Fivaz, R.; Mooser, E. Mobility of Charge Carriers In Semiconducting Layer Structures. *Phys. Rev.* **1967**, *163*, 743–755.
16. Radisavljevic, B.; Radenovic, A.; Brivio, J.; Giacometti, V.; Kis, A. Single-Layer MoS_2 Transistors. *Nat. Nanotechnol.* **2011**, *6*, 147–150.
17. Ye, J. T.; Zhang, Y. J.; Akashi, R.; Bahramy, M. S.; Arita, R.; Iwasa, Y. Superconducting Dome in a Gate-Tuned Band Insulator. *Science* **2012**, *338*, 1193–1196.
18. Withers, R. L.; Wilson, J. A. An Examination of the Formation and Characteristics of Charge-Density Waves in Inorganic Materials with Special Reference to the Two- and One-Dimensional Transition-Metal Chalcogenides. *J. Phys. C* **1986**, *19*, 4809–4845.
19. Zeng, Z.; Yin, Z.; Huang, X.; Li, H.; He, Q.; Lu, G.; Boey, F.; Zhang, H. Single-Layer Semiconducting Nanosheets: High-Yield Preparation and Device Fabrication. *Angew. Chem., Int. Ed.* **2011**, *50*, 11093–11097.
20. Zhu, Z.; Cheng, Y.; Schwingenschlögl, U. Topological Phase Diagrams of Bulk and Monolayer $TiS_{2-x}Te_x$. *Phys. Rev. Lett.* **2013**, *110*, 077202.
21. Song, H. S.; Li, S. L.; Gao, L.; Xu, Y.; Ueno, K.; Tang, J.; Cheng, Y. B.; Tsukagoshi, K. High-Performance Top-Gated Monolayer SnS_2 Field-Effect Transistors and Their Integrated Logic Circuits. *Nanoscale* **2013**, *5*, 9666–9670.
22. Zeng, Z.; Sun, T.; Zhu, J.; Huang, X.; Yin, Z.; Lu, G.; Fan, Z.; Yan, Q.; Hng, H. H.; Zhang, H. An Effective Method for the Fabrication of Few-Layer-Thick Inorganic Nanosheets. *Angew. Chem., Int. Ed.* **2012**, *51*, 9052–9056.
23. Zeng, Z.; Tan, C.; Huang, X.; Bao, S.; Zhang, H. Growth of Noble Metal Nanoparticles on Single-Layer TiS_2 and TaS_2 Nanosheets for Hydrogen Evolution Reaction. *Energy Environ. Sci.* **2014**, *7*, 797–803.
24. Hosono, H. Recent Progress in Transparent Oxide Semiconductors: Materials and Device Application. *Thin Solid Films* **2007**, *515*, 6000–6014.
25. Nomura, K.; Ohta, H.; Takagi, A.; Kamiya, T.; Hirano, M.; Hosono, H. Room-Temperature Fabrication of Transparent Flexible Thin-Film Transistors Using Amorphous Oxide Semiconductors. *Nature* **2004**, *432*, 488–492.
26. Guo, X.; Ortiz, R. P.; Zheng, Y.; Kim, M.-G.; Zhang, S.; Hu, Y.; Lu, G.; Facchetti, A.; Marks, T. J. Thieno[3,4-C] Pyrrole-4,6-Dione-Based Polymer Semiconductors: Toward High-Performance, Air-Stable Organic Thin-Film Transistors. *J. Am. Chem. Soc.* **2011**, *133*, 13685–13697.
27. Huang, H.; Chen, Z.; Ortiz, R. P.; Newman, C.; Usta, H.; Lou, S.; Youn, J.; Noh, Y.-Y.; Baeg, K.-J.; Chen, L. X.; *et al.* Combining Electron-Neutral Building Blocks with Intramolecular "Conformational Locks" Affords Stable, High-Mobility p- and n-Channel Polymer Semiconductors. *J. Am. Chem. Soc.* **2012**, *134*, 10966–10973.
28. Marks, T. J. Materials for Organic and Hybrid Inorganic/Organic Electronics. *MRS Bull.* **2010**, *35*, 1018–1027.
29. Ortiz, R. P.; Herrera, H.; Seoane, C.; Segura, J. L.; Facchetti, A.; Marks, T. J. Rational Design of Ambipolar Organic Semiconductors: Is Core Planarity Central to Ambipolarity in Thiophene–Naphthalene Semiconductors? *Chem.—Eur. J.* **2012**, *18*, 532–543.
30. Usta, H.; Facchetti, A.; Marks, T. J. n-Channel Semiconductor Materials Design for Organic Complementary Circuits. *Acc. Chem. Res.* **2011**, *44*, 501–510.
31. Liu, J.; Buchholz, D. B.; Chang, R. P. H.; Facchetti, A.; Marks, T. J. High-Performance Flexible Transparent Thin-Film Transistors Using a Hybrid Gate Dielectric and an Amorphous Zinc Indium Tin Oxide Channel. *Adv. Mater.* **2010**, *22*, 2333–2337.
32. Liu, J.; Buchholz, D. B.; Hennek, J. W.; Chang, R. P. H.; Facchetti, A.; Marks, T. J. All-Amorphous-Oxide Transparent, Flexible Thin-Film Transistors. Efficacy of Bilayer Gate Dielectrics. *J. Am. Chem. Soc.* **2010**, *132*, 11934–11942.
33. Liu, J.; Hennek, J. W.; Buchholz, D. B.; Ha, Y.-g.; Xie, S.; Dravid, V. P.; Chang, R. P. H.; Facchetti, A.; Marks, T. J. Reinforced Self-Assembled Nanodielectrics for High-Performance Transparent Thin Film Transistors. *Adv. Mater.* **2011**, *23*, 992–997.
34. Mattheiss, L. F. Band Structures of Transition-Metal-Dichalcogenide Layer Compounds. *Phys. Rev. B* **1973**, *8*, 3719–3740.
35. Podberezskaya, N. V.; Magarill, S. A.; Pervukhina, N. V.; Borisov, S. V. Crystal Chemistry of Dichalcogenides MX_2. *J. Struct. Chem.* **2001**, *42*, 654–681.
36. Xu, M.; Liang, T.; Shi, M.; Chen, H. Graphene-like Two-Dimensional Materials. *Chem. Rev.* **2013**, *113*, 3766–3798.
37. Eda, G.; Fujita, T.; Yamaguchi, H.; Voiry, D.; Chen, M.; Chhowalla, M. Coherent Atomic and Electronic

Heterostructures of Single-Layer MoS_2. *ACS Nano* **2012**, *6*, 7311–7317.
38. Eda, G.; Yamaguchi, H.; Voiry, D.; Fujita, T.; Chen, M.; Chhowalla, M. Photoluminescence from Chemically Exfoliated MoS_2. *Nano Lett.* **2011**, *11*, 5111–5116.
39. Novoselov, K.; Jiang, D.; Schedin, F.; Booth, T.; Khotkevich, V.; Morozov, S.; Geim, A. Two-Dimensional Atomic Crystals. *Proc. Natl. Acad. Sci. U.S.A.* **2005**, *102*, 10451–10453.
40. Li, H.; Lu, G.; Yin, Z.; He, Q.; Li, H.; Zhang, Q.; Zhang, H. Optical Identification of Single- and Few-Layer MoS_2 Sheets. *Small* **2012**, *8*, 682–686.
41. Late, D. J.; Liu, B.; Matte, H. S. S. R.; Rao, C. N. R.; Dravid, V. P. Rapid Characterization of Ultrathin Layers of Chalcogenides on SiO_2/Si Substrates. *Adv. Funct. Mater.* **2012**, *22*, 1894–1905.
42. Zheng, J.; Zhang, H.; Dong, S.; Liu, Y.; Tai Nai, C.; Suk Shin, H.; Young Jeong, H.; Liu, B.; Ping Loh, K. High Yield Exfoliation of Two-Dimensional Chalcogenides Using Sodium Naphthalenide. *Nat. Commun.* **2014**, *5*, 2995.
43. Gu, X.; Cui, W.; Li, H.; Wu, Z.; Zeng, Z.; Lee, S.-T.; Zhang, H.; Sun, B. A Solution-Processed Hole Extraction Layer Made from Ultrathin MoS_2 Nanosheets for Efficient Organic Solar Cells. *Adv. Energy Mater.* **2013**, *3*, 1262–1268.
44. Mak, K. F.; Lee, C.; Hone, J.; Shan, J.; Heinz, T. F. Atomically Thin MoS_2: A New Direct-Gap Semiconductor. *Phys. Rev. Lett.* **2010**, *105*, 136805.
45. Jin, W.; Yeh, P.-C.; Zaki, N.; Zhang, D.; Sadowski, J. T.; Al-Mahboob, A.; van der Zande, A. M.; Chenet, D. A.; Dadap, J. I.; Herman, I. P.; *et al.* Direct Measurement of the Thickness-Dependent Electronic Band Structure of MoS_2 Using Angle-Resolved Photoemission Spectroscopy. *Phys. Rev. Lett.* **2013**, *111*, 106801.
46. Kuc, A.; Zibouche, N.; Heine, T. Influence of Quantum Confinement on the Electronic Structure of the Transition Metal Sulfide TS_2. *Phys. Rev. B* **2011**, *83*, 245213.
47. Ellis, J. K.; Lucero, M. J.; Scuseria, G. E. The Indirect to Direct Band Gap Transition in Multilayered MoS_2 As Predicted by Screened Hybrid Density Functional Theory. *Appl. Phys. Lett.* **2011**, *99*, 261908.
48. Kadantsev, E. S.; Hawrylak, P. Electronic Structure of a Single MoS_2 Monolayer. *Solid State Commun.* **2012**, *152*, 909–913.
49. Cheiwchanchamnangij, T.; Lambrecht, W. R. Quasiparticle Band Structure Calculation of Monolayer, Bilayer, and Bulk MoS_2. *Phys. Rev. B* **2012**, *85*, 205302.
50. Splendiani, A.; Sun, L.; Zhang, Y.; Li, T.; Kim, J.; Chim, C.-Y.; Galli, G.; Wang, F. Emerging Photoluminescence in Monolayer MoS_2. *Nano Lett.* **2010**, *10*, 1271–1275.
51. Tongay, S.; Zhou, J.; Ataca, C.; Lo, K.; Matthews, T. S.; Li, J.; Grossman, J. C.; Wu, J. Thermally Driven Crossover from Indirect toward Direct Bandgap in 2D Semiconductors: $MoSe_2$ *versus* MoS_2. *Nano Lett.* **2012**, *12*, 5576–5580.
52. Zhao, W.; Ghorannevis, Z.; Chu, L.; Toh, M.; Kloc, C.; Tan, P.-H.; Eda, G. Evolution of Electronic Structure in Atomically Thin Sheets of WS_2 and WSe_2. *ACS Nano* **2012**, *7*, 791–797.
53. Ramasubramaniam, A. Large Excitonic Effects in Monolayers of Molybdenum and Tungsten Dichalcogenides. *Phys. Rev. B* **2012**, *86*, 115409.
54. Berkelbach, T. C.; Hybertsen, M. S.; Reichman, D. R. Theory of Neutral and Charged Excitons in Monolayer Transition Metal Dichalcogenides. *Phys. Rev. B* **2013**, *88*, 045318.
55. Mak, K. F.; He, K.; Lee, C.; Lee, G. H.; Hone, J.; Heinz, T. F.; Shan, J. Tightly Bound Trions in Monolayer MoS_2. *Nat. Mater.* **2012**, *12*, 207–211.
56. Ross, J. S.; Wu, S.; Yu, H.; Ghimire, N. J.; Jones, A. M.; Aivazian, G.; Yan, J.; Mandrus, D. G.; Xiao, D.; Yao, W.; *et al.* Electrical Control of Neutral and Charged Excitons in a Monolayer Semiconductor. *Nat. Commun.* **2013**, *4*, 1474.
57. Korn, T.; Heydrich, S.; Hirmer, M.; Schmutzler, J.; Schüller, C. Low-Temperature Photocarrier Dynamics in Monolayer MoS_2. *Appl. Phys. Lett.* **2011**, *99*, 102109.
58. Plechinger, G.; Schrettenbrunner, F. X.; Eroms, J.; Weiss, D.; Schüller, C.; Korn, T. Low-Temperature Photoluminescence of Oxide-Covered Single-Layer MoS_2. *Phys. Status Solidi Rapid Res. Lett.* **2012**, *6*, 126–128.
59. Conley, H. J.; Wang, B.; Ziegler, J. I.; Haglund, R. F.; Pantelides, S. T.; Bolotin, K. I. Bandgap Engineering of Strained Monolayer and Bilayer MoS_2. *Nano Lett.* **2013**, *13*, 3626–3630.
60. Castellanos-Gomez, A.; Roldán, R.; Cappelluti, E.; Buscema, M.; Guinea, F.; van der Zant, H. S. J.; Steele, G. A. Local Strain Engineering in Atomically Thin MoS_2. *Nano Lett.* **2013**, *13*, 5361–5366.
61. Xiao, D.; Liu, G.-B.; Feng, W.; Xu, X.; Yao, W. Coupled Spin and Valley Physics in Monolayers of MoS_2 and Other Group-VI Dichalcogenides. *Phys. Rev. Lett.* **2012**, *108*, 196802.
62. Gunawan, O.; Shkolnikov, Y. P.; Vakili, K.; Gokmen, T.; De Poortere, E. P.; Shayegan, M. Valley Susceptibility of an Interacting Two-Dimensional Electron System. *Phys. Rev. Lett.* **2006**, *97*, 186404.
63. Shkolnikov, Y. P.; De Poortere, E. P.; Tutuc, E.; Shayegan, M. Valley Splitting of AlAs Two-Dimensional Electrons in a Perpendicular Magnetic Field. *Phys. Rev. Lett.* **2002**, *89*, 226805.
64. Mak, K. F.; He, K.; Shan, J.; Heinz, T. F. Control of Valley Polarization in Monolayer MoS_2 by Optical Helicity. *Nat. Nanotechnol.* **2012**, *7*, 494–498.
65. Zeng, H.; Dai, J.; Yao, W.; Xiao, D.; Cui, X. Valley Polarization in MoS_2 Monolayers by Optical Pumping. *Nat. Nanotechnol.* **2012**, *7*, 490–493.
66. Cao, T.; Wang, G.; Han, W.; Ye, H.; Zhu, C.; Shi, J.; Niu, Q.; Tan, P.; Wang, E.; Liu, B.; *et al.* Valley-Selective Circular Dichroism of Monolayer Molybdenum Disulphide. *Nat. Commun.* **2012**, *3*, 887.
67. Jones, A. M.; Yu, H.; Ghimire, N. J.; Wu, S.; Aivazian, G.; Ross, J. S.; Zhao, B.; Yan, J.; Mandrus, D. G.; Xiao, D.; *et al.* Optical Generation of Excitonic Valley Coherence in Monolayer WSe_2. *Nat. Nanotechnol.* **2013**, *8*, 634–638.
68. Wu, S.; Ross, J. S.; Liu, G.-B.; Aivazian, G.; Jones, A.; Fei, Z.; Zhu, W.; Xiao, D.; Yao, W.; Cobden, D.; *et al.* Electrical Tuning of Valley Magnetic Moment Through Symmetry Control in Bilayer MoS_2. *Nat. Phys.* **2013**, *9*, 149–153.
69. Lee, C.; Yan, H.; Brus, L. E.; Heinz, T. F.; Hone, J.; Ryu, S. Anomalous Lattice Vibrations of Single- and Few-Layer MoS_2. *ACS Nano* **2010**, *4*, 2695–2700.
70. Li, H.; Zhang, Q.; Yap, C. C. R.; Tay, B. K.; Edwin, T. H. T.; Olivier, A.; Baillargeat, D. From Bulk to Monolayer MoS_2: Evolution of Raman Scattering. *Adv. Funct. Mater.* **2012**, *22*, 1385–1390.
71. Najmaei, S.; Liu, Z.; Ajayan, P. M.; Lou, J. Thermal Effects on the Characteristic Raman Spectrum of Molybdenum Disulfide (MoS_2) of Varying Thicknesses. *Appl. Phys. Lett.* **2012**, *100*, 013106.
72. Lanzillo, N. A.; Birdwell, A. G.; Amani, M.; Crowne, F. J.; Shah, P. B.; Najmaei, S.; Liu, Z.; Ajayan, P. M.; Lou, J.; Dubey, M.; *et al.* Temperature-Dependent Phonon Shifts in Monolayer MoS_2. *Appl. Phys. Lett.* **2013**, *103*, 093102.
73. Marulasiddappa, T.; Late, D. J. Temperature Dependent Phonon Shifts in Single-Layer WS_2. *ACS Appl. Mater. Interfaces* **2013**, *6*, 1158–1163.
74. Chakraborty, B.; Bera, A.; Muthu, D. V. S.; Bhowmick, S.; Waghmare, U. V.; Sood, A. K. Symmetry-Dependent Phonon Renormalization in Monolayer MoS_2 Transistor. *Phys. Rev. B* **2012**, *85*, 161403.
75. Berkdemir, A.; Gutierrez, H. R.; Botello-Mendez, A. R.; Perea-Lopez, N.; Elias, A. L.; Chia, C.-I.; Wang, B.; Crespi, V. H.; Lopez-Urias, F.; Charlier, J.-C.; *et al.* Identification of Individual and Few Layers of WS_2 Using Raman Spectroscopy. *Sci. Rep.* **2013**, 3.
76. Grant, A.; Griffiths, T.; Pitt, G.; Yoffe, A. The Electrical Properties and the Magnitude of the Indirect Gap in the Semiconducting Transition Metal Dichalcogenide Layer Crystals. *J. Phys. C* **1975**, *8*, L17–L23.
77. Podzorov, V.; Gershenson, M.; Kloc, C.; Zeis, R.; Bucher, E. High-Mobility Field-Effect Transistors Based on Transition Metal Dichalcogenides. *Appl. Phys. Lett.* **2004**, *84*, 3301–3303.

78. Novoselov, K. S.; Geim, A. K.; Morozov, S.; Jiang, D.; Zhang, Y.; Dubonos, S.; Grigorieva, I.; Firsov, A. Electric Field Effect in Atomically Thin Carbon Films. *Science* **2004**, *306*, 666–669.
79. Radisavljevic, B.; Kis, A. Reply to "Measurement of Mobility in Dual-Gated MoS_2 Transistors". *Nat. Nanotechnol.* **2013**, *8*, 147–148.
80. Radisavljevic, B.; Kis, A. Mobility Engineering and Metal-Insulator Transition in Monolayer MoS_2. *Nat. Mater.* **2013**, *12*, 815–820.
81. Fuhrer, M. S.; Hone, J. Measurement of Mobility in Dual-Gated MoS_2 Transistors. *Nat. Nanotechnol.* **2013**, *8*, 146–147.
82. Jariwala, D.; Sangwan, V. K.; Late, D. J.; Johns, J. E.; Dravid, V. P.; Marks, T. J.; Lauhon, L. J.; Hersam, M. C. Band-like Transport in High Mobility Unencapsulated Single-Layer MoS_2 Transistors. *Appl. Phys. Lett.* **2013**, *102*, 173107.
83. Sangwan, V. K.; Arnold, H. N.; Jariwala, D.; Marks, T. J.; Lauhon, L. J.; Hersam, M. C. Low-Frequency Electronic Noise in Single-Layer MoS_2 Transistors. *Nano Lett.* **2013**, *13*, 4351–4355.
84. Zhang, W.; Huang, J.-K.; Chen, C.-H.; Chang, Y.-H.; Cheng, Y.-J.; Li, L.-J. High-Gain Phototransistors Based on a CVD MoS_2 Monolayer. *Adv. Mater.* **2013**, *25*, 3456–3461.
85. Perera, M. M.; Lin, M.-W.; Chuang, H.-J.; Chamlagain, B. P.; Wang, C.; Tan, X.; Cheng, M. M.-C.; Tománek, D.; Zhou, Z. Improved Carrier Mobility in Few-Layer MoS_2 Field-Effect Transistors with Ionic-Liquid Gating. *ACS Nano* **2013**, *7*, 4449–4458.
86. Liu, H.; Ye, P. D. MoS_2 Dual-Gate MOSFET with Atomic-Layer-Deposited Al_2O_3 as Top-Gate Dielectric. *IEEE Electron Device Lett.* **2011**, *33*, 546–548.
87. Lin, M.-W.; Liu, L.; Lan, Q.; Tan, X.; Dhindsa, K. S.; Zeng, P.; Naik, V. M.; Cheng, M. M.-C.; Zhou, Z. Mobility Enhancement and Highly Efficient Gating of Monolayer MoS_2 Transistors with Polymer Electrolyte. *J. Phys. D* **2012**, *45*, 345102.
88. Bao, W.; Cai, X.; Kim, D.; Sridhara, K.; Fuhrer, M. S. High Mobility Ambipolar MoS_2 Field-Effect Transistors: Substrate and Dielectric Effects. *Appl. Phys. Lett.* **2013**, *102*, 042104.
89. Lee, G.-H.; Yu, Y.-J.; Cui, X.; Petrone, N.; Lee, C.-H.; Choi, M. S.; Lee, D.-Y.; Lee, C.; Yoo, W. J.; Watanabe, K.; *et al.* Flexible and Transparent MoS_2 Field-Effect Transistors on Hexagonal Boron Nitride-Graphene Heterostructures. *ACS Nano* **2013**, *7*, 7931–7936.
90. Li, Y.; Xu, C.-Y.; Hu, P.; Zhen, L. Carrier Control of MoS_2 Nanoflakes by Functional Self-Assembled Monolayers. *ACS Nano* **2013**, *7*, 7795–7804.
91. Chan, M. Y.; Komatsu, K.; Li, S.-L.; Xu, Y.; Darmawan, P.; Kuramochi, H.; Nakaharai, S.; Aparecido-Ferreira, A.; Watanabe, K.; Taniguchi, T.; *et al.* Suppression of Thermally Activated Carrier Transport in Atomically Thin MoS_2 on Crystalline Hexagonal Boron Nitride Substrates. *Nanoscale* **2013**, *5*, 9572–9576.
92. Jin, T.; Kang, J.; Su Kim, E.; Lee, S.; Lee, C. Suspended Single-Layer MoS_2 Devices. *J. Appl. Phys.* **2013**, *114*, 164509.
93. Cho, K.; Park, W.; Park, J.; Jeong, H.; Jang, J.; Kim, T.-Y.; Hong, W.-K.; Hong, S.; Lee, T. Electric Stress-Induced Threshold Voltage Instability of Multilayer MoS_2 Field Effect Transistors. *ACS Nano* **2013**, *7*, 7751–7758.
94. Braga, D.; Gutiérrez Lezama, I.; Berger, H.; Morpurgo, A. F. Quantitative Determination of the Band Gap of WS_2 with Ambipolar Ionic Liquid-Gated Transistors. *Nano Lett.* **2012**, *12*, 5218–5223.
95. Zhang, Y.; Ye, J.; Matsuhashi, Y.; Iwasa, Y. Ambipolar MoS_2 Thin Flake Transistors. *Nano Lett.* **2012**, *12*, 1136–1140.
96. Das, S.; Appenzeller, J. Where Does the Current Flow in Two-Dimensional Layered Systems? *Nano Lett.* **2013**, *13*, 3396–3402.
97. Li, S.-L.; Wakabayashi, K.; Xu, Y.; Nakaharai, S.; Komatsu, K.; Li, W.-W.; Lin, Y.-F.; Aparecido-Ferreira, A.; Tsukagoshi, K. Thickness-Dependent Interfacial Coulomb Scattering in Atomically Thin Field-Effect Transistors. *Nano Lett.* **2013**, *13*, 3546–3552.
98. Ghatak, S.; Pal, A. N.; Ghosh, A. Nature of Electronic States in Atomically Thin MoS_2 Field-Effect Transistors. *ACS Nano* **2011**, *5*, 7707–7712.
99. Das, S.; Chen, H.-Y.; Penumatcha, A. V.; Appenzeller, J. High Performance Multilayer MoS_2 Transistors with Scandium Contacts. *Nano Lett.* **2012**, *13*, 100–105.
100. Kim, S.; Konar, A.; Hwang, W. S.; Lee, J. H.; Lee, J.; Yang, J.; Jung, C.; Kim, H.; Yoo, J. B.; Choi, J. Y.; *et al.* High-Mobility and Low-Power Thin-Film Transistors Based on Multilayer MoS_2 Crystals. *Nat. Commun.* **2012**, *3*, 1011.
101. Ayari, A.; Cobas, E.; Ogundadegbe, O.; Fuhrer, M. S. Realization and Electrical Characterization of Ultrathin Crystals of Layered Transition-Metal Dichalcogenides. *J. Appl. Phys.* **2007**, *101*, 014507.
102. Baugher, B.; Churchill, H. O.; Yang, Y.; Jarillo-Herrero, P. Intrinsic Electronic Transport Properties of High Quality Monolayer and Bilayer MoS_2. *Nano Lett.* **2013**, *13*, 4212–4216.
103. Neal, A. T.; Liu, H.; Gu, J.; Ye, P. D. Magneto-Transport in MoS_2: Phase Coherence, Spin Orbit Scattering and the Hall Factor. *ACS Nano* **2013**, *7*, 7077–7082.
104. Larentis, S.; Fallahazad, B.; Tutuc, E. Field-Effect Transistors and Intrinsic Mobility in Ultra-thin $MoSe_2$ Layers. *Appl. Phys. Lett.* **2012**, *101*, 223104.
105. Kaasbjerg, K.; Thygesen, K. S.; Jacobsen, K. W. Phonon-Limited Mobility in n-Type Single-Layer MoS_2 from First Principles. *Phys. Rev. B* **2012**, *85*, 115317.
106. Ong, Z.-Y.; Fischetti, M. V. Mobility Enhancement and Temperature Dependence in Top-Gated Single-Layer MoS_2. *Phys. Rev. B* **2013**, *88*, 165316.
107. Li, X.; Mullen, J. T.; Jin, Z.; Borysenko, K. M.; Buongiorno Nardelli, M.; Kim, K. W. Intrinsic Electrical Transport Properties of Monolayer Silicene and MoS_2 from First Principles. *Phys. Rev. B* **2013**, *87*, 115418.
108. Kaasbjerg, K.; Thygesen, K. S.; Jauho, A.-P. Acoustic Phonon-Limited Mobility in Two-Dimensional Semiconductors: Deformation Potential and Piezoelectric Scattering in Monolayer MoS_2 from First Principles. *Phys. Rev. B* **2013**, *87*, 235312.
109. Zeng, L.; Xin, Z.; Chen, S.; Du, G.; Kang, J.; Liu, X. Remote Phonon and Impurity Screening Effect of Substrate and Gate Dielectric on Electron Dynamics in Single Layer MoS_2. *Appl. Phys. Lett.* **2013**, *103*, 113505.
110. Chen, J.-H.; Jang, C.; Xiao, S.; Ishigami, M.; Fuhrer, M. S. Intrinsic and Extrinsic Performance Limits of Graphene Devices on SiO_2. *Nat. Nanotechnol.* **2008**, *3*, 206–209.
111. Ma, N.; Jena, D. Charge Scattering and Mobility in Atomically Thin Semiconductors. *arXiv:1310.7157* **2013**.
112. Lembke, D.; Kis, A. Breakdown of High-Performance Monolayer MoS_2 Transistors. *ACS Nano* **2012**, *6*, 10070–10075.
113. Ghatak, S.; Ghosh, A. Observation of Trap-Assisted Space Charge Limited Conductivity in Short Channel MoS_2 Transistor. *Appl. Phys. Lett.* **2013**, *103*, 122103.
114. Fiori, G.; Szafranek, B. N.; Iannaccone, G.; Neumaier, D. Velocity Saturation in Few-Layer MoS_2 Transistor. *Appl. Phys. Lett.* **2013**, *103*, 233509.
115. Kim, S. K.; Xuan, Y.; Ye, P. D.; Mohammadi, S.; Back, J. H.; Shim, M. Atomic Layer Deposited Al_2O_3 for Gate Dielectric and Passivation Layer of Single-Walled Carbon Nanotube Transistors. *Appl. Phys. Lett.* **2007**, *90*, 163108.
116. Buscema, M.; Barkelid, M.; Zwiller, V.; van der Zant, H. S.; Steele, G. A.; Castellanos-Gomez, A. Large and Tunable Photothermoelectric Effect in Single-Layer MoS_2. *Nano Lett.* **2013**, *13*, 358–363.
117. Popov, I.; Seifert, G.; Tománek, D. Designing Electrical Contacts to MoS_2 Monolayers: A Computational Study. *Phys. Rev. Lett.* **2012**, *108*, 156802.
118. Liu, W.; Kang, J.; Sarkar, D.; Khatami, Y.; Jena, D.; Banerjee, K. Role of Metal Contacts in Designing High-Performance Monolayer n-Type WSe_2 Field Effect Transistors. *Nano Lett.* **2013**, *13*, 1983–1990.
119. Liu, D.; Guo, Y.; Fang, L.; Robertson, J. Sulfur Vacancies in Monolayer MoS_2 and Its Electrical Contacts. *Appl. Phys. Lett.* **2013**, *103*, 183113.

120. Liu, H.; Si, M.; Deng, Y.; Neal, A. T.; Du, Y.; Najmaei, S.; Ajayan, P. M.; Lou, J.; Ye, P. D. Switching Mechanism in Single-Layer Molybdenum Disulfide Transistors: An Insight into Current Flow across Schottky Barriers. *ACS Nano* **2014**, *8*, 1031–1038.
121. Walia, S.; Balendhran, S.; Wang, Y.; Ab Kadir, R.; Zoolfakar, A. S.; Atkin, P.; Ou, J. Z.; Sriram, S.; Kalantar-zadeh, K.; Bhaskaran, M. Characterization of Metal Contacts for Two-Dimensional MoS_2 Nanoflakes. *Appl. Phys. Lett.* **2013**, *103*, 232105.
122. Gong, C.; Huang, C.; Miller, J.; Cheng, L.; Hao, Y.; Cobden, D.; Kim, J.; Ruoff, R. S.; Wallace, R. M.; Cho, K.; *et al.* Metal Contacts on Physical Vapor Deposited Monolayer MoS_2. *ACS Nano* **2013**, *7*, 11350–11357.
123. Chen, J.-R.; Odenthal, P. M.; Swartz, A.; Floyd, G. C.; Wen, H.; Luo, K. Y.; Kawakami, R. K. Control of Schottky Barriers in Single Layer MoS_2 Transistors with Ferromagnetic Contacts. *Nano Lett.* **2013**, *13*, 3106–3110.
124. Dankert, A.; Langouche, L.; Kamalakar, M. V.; Dash, S. P. High-Performance Molybdenum Disulfide Field-Effect Transistors with Spin Tunnel Contacts. *ACS Nano* **2014**, *8*, 476–482.
125. Fang, H.; Chuang, S.; Chang, T. C.; Takei, K.; Takahashi, T.; Javey, A. High-Performance Single Layered WSe_2 p-FETs with Chemically Doped Contacts. *Nano Lett.* **2012**, *12*, 3788–3792.
126. Fang, H.; Tosun, M.; Seol, G.; Chang, T. C.; Takei, K.; Guo, J.; Javey, A. Degenerate n-Doping of Few-Layer Transition Metal Dichalcogenides by Potassium. *Nano Lett.* **2013**, *13*, 1991–1995.
127. Du, Y.; Liu, H.; Neal, A. T.; Si, M.; Ye, P. D. Molecular Doping of Multilayer MoS_2 Field-Effect Transistors: Reduction in Sheet and Contact Resistances. *IEEE Electron Device Lett.* **2013**, *34*, 1328–1330.
128. Liu, H.; Si, M.; Najmaei, S.; Neal, A. T.; Du, Y.; Ajayan, P. M.; Lou, J.; Ye, P. D. Statistical Study of Deep Submicron Dual-Gated Field-Effect Transistors on Monolayer Chemical Vapor Deposition Molybdenum Disulfide Films. *Nano Lett.* **2013**, *13*, 2640–2646.
129. Liu, H.; Neal, A. T.; Ye, P. D. Channel Length Scaling of MoS_2 MOSFETs. *ACS Nano* **2012**, *6*, 8563–8569.
130. Yoon, Y.; Ganapathi, K.; Salahuddin, S. How Good Can Monolayer MoS_2 Transistors Be? *Nano Lett.* **2011**, *11*, 3768–3773.
131. Leitao, L.; Bala Kumar, S.; Yijian, O.; Guo, J. Performance Limits of Monolayer Transition Metal Dichalcogenide Transistors. *IEEE Trans. Electron Devices* **2011**, *58*, 3042–3047.
132. Liu, L.; Lu, Y.; Guo, J. On Monolayer MoS_2 Field-Effect Transistors at the Scaling Limit. *IEEE Trans. Electron Devices* **2013**, *60*, 4133–4139.
133. Pradhan, N. R.; Rhodes, D.; Zhang, Q.; Talapatra, S.; Terrones, M.; Ajayan, P. M.; Balicas, L. Intrinsic Carrier Mobility of Multi-Layered MoS_2 Field-Effect Transistors on SiO_2. *Appl. Phys. Lett.* **2013**, *102*, 123105.
134. Everaerts, K.; Zeng, L.; Hennek, J. W.; Camacho, D. I.; Jariwala, D.; Bedzyk, M. J.; Hersam, M. C.; Marks, T. J. Printed Indium Gallium Zinc Oxide Transistors. Self-Assembled Nanodielectric Effects on Low-Temperature Combustion Growth and Carrier Mobility. *ACS Appl. Mater. Interfaces* **2013**, *5*, 11884–11893.
135. Ha, Y.-G.; Everaerts, K.; Hersam, M. C.; Marks, T. J. Hybrid Gate Dielectric Materials for Unconventional Electronic Circuitry. *Acc. Chem. Res.* **2014**, 10.1021/ar4002262.
136. Sangwan, V. K.; Ortiz, R. P.; Alaboson, J. M. P.; Emery, J. D.; Bedzyk, M. J.; Lauhon, L. J.; Marks, T. J.; Hersam, M. C. Fundamental Performance Limits of Carbon Nanotube Thin-Film Transistors Achieved Using Hybrid Molecular Dielectrics. *ACS Nano* **2012**, *6*, 7480–7488.
137. Everaerts, K.; Emery, J. D.; Jariwala, D.; Karmel, H. J.; Sangwan, V. K.; Prabhumirashi, P. L.; Geier, M. L.; McMorrow, J. J. E.; Bedzyk, M. J.; Facchetti, A.; *et al.* Ambient-Processable High-Capacitance Hafnia-Organic Self-Assembled Nanodielectrics. *J. Am. Chem. Soc.* **2013**, *135*, 8926–8939.
138. Chang, H.-Y.; Yang, S.; Lee, J.; Tao, L.; Hwang, W.-S.; Jena, D.; Lu, N.; Akinwande, D. High-Performance, Highly Bendable MoS_2 Transistors with High-K Dielectrics for Flexible Low-Power Systems. *ACS Nano* **2013**, *7*, 5446–5452.
139. Salvatore, G. A.; Münzenrieder, N.; Barraud, C.; Petti, L.; Zysset, C.; Büthe, L.; Ensslin, K.; Tröster, G. Fabrication and Transfer of Flexible Few-Layers MoS_2 Thin Film Transistors to Any Arbitrary Substrate. *ACS Nano* **2013**, *7*, 8809–8815.
140. Pu, J.; Yomogida, Y.; Liu, K.-K.; Li, L.-J.; Iwasa, Y.; Takenobu, T. Highly Flexible MoS_2 Thin-Film Transistors with Ion Gel Dielectrics. *Nano Lett.* **2012**, *12*, 4013–4017.
141. Radisavljevic, B.; Whitwick, M. B.; Kis, A. Integrated Circuits and Logic Operations Based on Single-Layer MoS_2. *ACS Nano* **2011**, *5*, 9934–9938.
142. Wang, H.; Yu, L.; Lee, Y.-H.; Shi, Y.; Hsu, A.; Chin, M. L.; Li, L.-J.; Dubey, M.; Kong, J.; Palacios, T. Integrated Circuits Based on Bilayer MoS_2 Transistors. *Nano Lett.* **2012**, *12*, 4674–4680.
143. Wang, H.; Yu, L.; Lee, Y.; Fang, W.; Hsu, A.; Herring, P.; Chin, M.; Dubey, M.; Li, L.; Kong, J.; *et al.* In *Large-Scale 2-D Electronics Based on Single-Layer MoS_2 Grown by Chemical Vapor Deposition*; Electron Devices Meeting (IEDM), IEEE International, **2012**; pp 4.6.1−4.6.4.
144. Huang, J.-K.; Pu, J.; Hsu, C.-L.; Chiu, M.-H.; Juang, Z.-Y.; Chang, Y.-H.; Chang, W.-H.; Iwasa, Y.; Takenobu, T.; Li, L.-J. Large-Area Synthesis of Highly Crystalline WSe_2 Monolayers and Device Applications. *ACS Nano* **2014**, *8*, 923–930.
145. Guerriero, E.; Polloni, L.; Bianchi, M.; Behnam, A.; Carrion, E.; Rizzi, L. G.; Pop, E.; Sordan, R. Gigahertz Integrated Graphene Ring Oscillators. *ACS Nano* **2013**, *7*, 5588–5594.
146. Chen, Z.; Appenzeller, J.; Lin, Y.-M.; Sippel-Oakley, J.; Rinzler, A. G.; Tang, J.; Wind, S. J.; Solomon, P. M.; Avouris, P. An Integrated Logic Circuit Assembled on a Single Carbon Nanotube. *Science* **2006**, *311*, 1735.
147. Klauk, H.; Halik, M.; Zschieschang, U.; Eder, F.; Schmid, G.; Dehm, C. Pentacene Organic Transistors and Ring Oscillators on Glass and on Flexible Polymeric Substrates. *Appl. Phys. Lett.* **2003**, *82*, 4175–4177.
148. Na, J. H.; Kitamura, M.; Arakawa, Y. Organic/Inorganic Hybrid Complementary Circuits Based on Pentacene and Amorphous Indium Gallium Zinc Oxide Transistors. *Appl. Phys. Lett.* **2008**, *93*, 213505.
149. Hayashi, R.; Ofuji, M.; Kaji, N.; Takahashi, K.; Abe, K.; Yabuta, H.; Sano, M.; Kumomi, H.; Nomura, K.; Kamiya, T.; *et al.* Circuits Using Uniform TFTs Based on Amorphous-In-Ga-Zn-O. *J. Soc. Inf. Disp.* **2007**, *15*, 915–921.
150. Lee, Y.-H.; Zhang, X.-Q.; Zhang, W.; Chang, M.-T.; Lin, C.-T.; Chang, K.-D.; Yu, Y.-C.; Wang, J. T.-W.; Chang, C.-S.; Li, L.-J.; *et al.* Synthesis of Large-Area MoS_2 Atomic Layers with Chemical Vapor Deposition. *Adv. Mater.* **2012**, *24*, 2320–2325.
151. Liu, K.-K.; Zhang, W.; Lee, Y.-H.; Lin, Y.-C.; Chang, M.-T.; Su, C.-Y.; Chang, C.-S.; Li, H.; Shi, Y.; Zhang, H.; *et al.* Growth of Large-Area and Highly Crystalline MoS_2 Thin Layers on Insulating Substrates. *Nano Lett.* **2012**, *12*, 1538–1544.
152. Najmaei, S.; Liu, Z.; Zhou, W.; Zou, X.; Shi, G.; Lei, S.; Yakobson, B. I.; Idrobo, J.-C.; Ajayan, P. M.; Lou, J. Vapour Phase Growth and Grain Boundary Structure of Molybdenum Disulphide Atomic Layers. *Nat. Mater.* **2013**, *12*, 754–759.
153. van der Zande, A. M.; Huang, P. Y.; Chenet, D. A.; Berkelbach, T. C.; You, Y.; Lee, G.-H.; Heinz, T. F.; Reichman, D. R.; Muller, D. A.; Hone, J. C. Grains and Grain Boundaries in Highly Crystalline Monolayer Molybdenum Disulphide. *Nat. Mater.* **2013**, *12*, 554–561.
154. Amani, M.; Chin, M. L.; Birdwell, A. G.; O'Regan, T. P.; Najmaei, S.; Liu, Z.; Ajayan, P. M.; Lou, J.; Dubey, M. Electrical Performance of Monolayer MoS_2 Field-Effect Transistors Prepared by Chemical Vapor Deposition. *Appl. Phys. Lett.* **2013**, *102*, 193107.
155. Zhan, Y.; Liu, Z.; Najmaei, S.; Ajayan, P. M.; Lou, J. Large-Area Vapor-Phase Growth and Characterization of MoS_2 Atomic Layers on a SiO_2 Substrate. *Small* **2012**, *8*, 966–971.

156. Zhu, W.; Low, T.; Lee, Y.-H.; Wang, H.; Farmer, D. B.; Kong, J.; Xia, F.; Avouris, P. Electronic Transport and Device Prospects of Monolayer Molybdenum Disulphide Grown by Chemical Vapour Deposition. *Nat. Commun.* **2014**, *5*, 3087.
157. Geier, M. L.; Prabhumirashi, P. L.; McMorrow, J. J.; Xu, W.; Seo, J.-W. T.; Everaerts, K.; Kim, C. H.; Marks, T. J.; Hersam, M. C. Subnanowatt Carbon Nanotube Complementary Logic Enabled by Threshold Voltage Control. *Nano Lett.* **2013**, *13*, 4810–4814.
158. Hafez, W.; Snodgrass, W.; Feng, M. 12.5nm Base Pseudomorphic Heterojunction Bipolar Transistors Achieving F_t = 710 GHz and F_{max} = 340 GHz. *Appl. Phys. Lett.* **2005**, *87*, 252109.
159. Nguyen, L. D.; Brown, A. S.; Thompson, M. A.; Jelloian, L. M. 50nm Self-Aligned-Gate Pseudomorphic AlInAs/GaInAs High Electron Mobility Transistors. *IEEE Trans. Electron Devices* **1992**, *39*, 2007–2014.
160. Georgiou, T.; Jalil, R.; Belle, B. D.; Britnell, L.; Gorbachev, R. V.; Morozov, S. V.; Kim, Y.-J.; Gholinia, A.; Haigh, S. J.; Makarovsky, O.; *et al.* Vertical Field-Effect Transistor Based on Graphene-WS_2 Heterostructures for Flexible and Transparent Electronics. *Nat. Nanotechnol.* **2013**, *8*, 100–103.
161. Yang, H.; Heo, J.; Park, S.; Song, H. J.; Seo, D. H.; Byun, K.-E.; Kim, P.; Yoo, I.; Chung, H.-J.; Kim, K. Graphene Barristor, a Triode Device with a Gate-Controlled Schottky Barrier. *Science* **2012**, *336*, 1140–1143.
162. Britnell, L.; Gorbachev, R.; Geim, A.; Ponomarenko, L.; Mishchenko, A.; Greenaway, M.; Fromhold, T.; Novoselov, K.; Eaves, L. Resonant Tunnelling and Negative Differential Conductance in Graphene Transistors. *Nat. Commun.* **2013**, *4*, 1794.
163. Britnell, L.; Gorbachev, R. V.; Jalil, R.; Belle, B. D.; Schedin, F.; Mishchenko, A.; Georgiou, T.; Katsnelson, M. I.; Eaves, L.; Morozov, S. V.; *et al.* Field-Effect Tunneling Transistor Based on Vertical Graphene Heterostructures. *Science* **2012**, *335*, 947–950.
164. Myoung, N.; Seo, K.; Lee, S. J.; Ihm, G. Large Current Modulation and Spin-Dependent Tunneling of Vertical Graphene/MoS_2 Heterostructures. *ACS Nano* **2013**, *7*, 7021–7027.
165. Yu, W. J.; Li, Z.; Zhou, H.; Chen, Y.; Wang, Y.; Huang, Y.; Duan, X. Vertically Stacked Multi-Heterostructures of Layered Materials for Logic Transistors and Complementary Inverters. *Nat. Mater.* **2012**, *12*, 246–252.
166. Bertolazzi, S.; Krasnozhon, D.; Kis, A. Nonvolatile Memory Cells Based on MoS_2/Graphene Heterostructures. *ACS Nano* **2013**, *7*, 3246–3252.
167. Choi, M. S.; Lee, G.-H.; Yu, Y.-J.; Lee, D.-Y.; Lee, S. H.; Kim, P.; Hone, J.; Yoo, W. J. Controlled Charge Trapping by Molybdenum Disulphide and Graphene in Ultrathin Heterostructured Memory Devices. *Nat. Commun.* **2013**, *4*, 1624.
168. Lee, H. S.; Min, S.-W.; Park, M. K.; Lee, Y. T.; Jeon, P. J.; Kim, J. H.; Ryu, S.; Im, S. MoS_2 Nanosheets for Top-Gate Nonvolatile Memory Transistor Channel. *Small* **2012**, *8*, 3111–3115.
169. Liu, J.; Zeng, Z.; Cao, X.; Lu, G.; Wang, L.-H.; Fan, Q.-L.; Huang, W.; Zhang, H. Preparation of MoS_2-Polyvinylpyrrolidone Nanocomposites for Flexible Nonvolatile Rewritable Memory Devices with Reduced Graphene Oxide Electrodes. *Small* **2012**, *8*, 3517–3522.
170. Yin, Z.; Zeng, Z.; Liu, J.; He, Q.; Chen, P.; Zhang, H. Memory Devices Using a Mixture of MoS_2 and Graphene Oxide as the Active Layer. *Small* **2013**, *9*, 727–731.
171. Spah, R.; Lux-Steiner, M.; Obergfell, M.; Bucher, E.; Wagner, S. n-$MoSe_2$/p-WSe_2 Heterojunctions. *Appl. Phys. Lett.* **1985**, *47*, 871–873.
172. Spah, R.; Elrod, U.; Lux-Steiner, M.; Bucher, E.; Wagner, S. p-n Junctions in Tungsten Diselenide. *Appl. Phys. Lett.* **1983**, *43*, 79–81.
173. Jariwala, D.; Sangwan, V. K.; Wu, C.-C.; Prabhumirashi, P. L.; Geier, M. L.; Marks, T. J.; Lauhon, L. J.; Hersam, M. C. Gate-Tunable Carbon Nanotube–MoS_2 Heterojunction p-n Diode. *Proc. Natl. Acad. Sci. U.S.A.* **2013**, *110*, 18076–18080.
174. Chuang, S.; Kapadia, R.; Fang, H.; Chang, T. C.; Yen, W.-C.; Chueh, Y.-L.; Javey, A. Near-Ideal Electrical Properties of InAs/WSe_2 van der Waals Heterojunction Diodes. *Appl. Phys. Lett.* **2013**, *102*, 242101.
175. Ma, N.; Jena, D. Interband Tunneling in Two-Dimensional Crystal Semiconductors. *Appl. Phys. Lett.* **2013**, *102*, 132102.
176. Ghosh, R. K.; Mahapatra, S. Direct Band-to-Band Tunneling in Reverse Biased MoS_2 Nanoribbon p-n Junctions. *IEEE Trans. Electron Devices* **2013**, *60*, 274–279.
177. Zhang, Y. J.; Ye, J. T.; Yomogida, Y.; Takenobu, T.; Iwasa, Y. Formation of a Stable p–n Junction in a Liquid-Gated MoS_2 Ambipolar Transistor. *Nano Lett.* **2013**, *13*, 3023–3028.
178. Nam, H.; Wi, S.; Rokni, H.; Chen, M.; Priessnitz, G.; Lu, W.; Liang, X. MoS_2 Transistors Fabricated *via* Plasma-Assisted Nanoprinting of Few-Layer MoS_2 Flakes into Large-Area Arrays. *ACS Nano* **2013**, *7*, 5870–5881.
179. Chen, M.; Nam, H.; Wi, S.; Ji, L.; Ren, X.; Bian, L.; Lu, S.; Liang, X. Stable Few-Layer MoS_2 Rectifying Diodes Formed by Plasma-Assisted Doping. *Appl. Phys. Lett.* **2013**, *103*, 142110.
180. Chen, Y.; Xi, J.; Dumcenco, D. O.; Liu, Z.; Suenaga, K.; Wang, D.; Shuai, Z.; Huang, Y.-S.; Xie, L. Tunable Band Gap Photoluminescence from Atomically Thin Transition-Metal Dichalcogenide Alloys. *ACS Nano* **2013**, *7*, 4610–4616.
181. Mann, J.; Ma, Q.; Odenthal, P. M.; Isarraraz, M.; Le, D.; Preciado, E.; Barroso, D.; Yamaguchi, K.; von Son Palacio, G.; Nguyen, A.; *et al.* 2-Dimensional Transition Metal Dichalcogenides with Tunable Direct Band Gaps: $MoS_{2(1-x)}Se_{2x}$ Monolayers. *Adv. Mater.* **2014**, 10.1002/adma.201304389.
182. Chen, Y.; Dumcenco, D. O.; Zhu, Y.; Zhang, X.; Mao, N.; Feng, Q.; Zhang, M.; Zhang, J.; Tan, P.; Huang, Y.-S.; *et al.* Composition-Dependent Raman Modes of $Mo_{1-x}W_xS_2$ Monolayer Alloys. *Nanoscale* **2014**, 10.1039/C1033NR05630A.
183. Gong, Y.; Liu, Z.; Lupini, A. R.; Shi, G.; Lin, J.; Najmaei, S.; Lin, Z.; Elías, A. L.; Berkdemir, A.; You, G.; *et al.* Band Gap Engineering and Layer-by-Layer Mapping of Selenium-Doped Molybdenum Disulfide. *Nano Lett.* **2014**, 10.1021/nl4032296.
184. Xu, X.; Gabor, N. M.; Alden, J. S.; van der Zande, A. M.; McEuen, P. L. Photo-thermoelectric Effect at a Graphene Interface Junction. *Nano Lett.* **2010**, *10*, 562–566.
185. Liu, Y.; Nan, H.; Wu, X.; Pan, W.; Wang, W.; Bai, J.; Zhao, W.; Sun, L.; Wang, X.; Ni, Z. Layer-by-Layer Thinning of MoS_2 by Plasma. *ACS Nano* **2013**, *7*, 4202–4209.
186. Castellanos-Gomez, A.; Barkelid, M.; Goossens, A. M.; Calado, V. E.; van der Zant, H. S. J.; Steele, G. A. Laser-Thinning of MoS_2: On Demand Generation of a Single-Layer Semiconductor. *Nano Lett.* **2012**, *12*, 3187–3192.
187. Wu, J.; Li, H.; Yin, Z.; Li, H.; Liu, J.; Cao, X.; Zhang, Q.; Zhang, H. Layer Thinning and Etching of Mechanically Exfoliated MoS_2 Nanosheets by Thermal Annealing in Air. *Small* **2013**, *9*, 3314–3319.
188. Yin, Z.; Li, H.; Li, H.; Jiang, L.; Shi, Y.; Sun, Y.; Lu, G.; Zhang, Q.; Chen, X.; Zhang, H. Single-Layer MoS_2 Phototransistors. *ACS Nano* **2012**, *6*, 74–80.
189. Choi, W.; Cho, M. Y.; Konar, A.; Lee, J. H.; Cha, G. B.; Hong, S. C.; Kim, S.; Kim, J.; Jena, D.; Joo, J.; *et al.* High-Detectivity Multilayer MoS_2 Phototransistors with Spectral Response from Ultraviolet to Infrared. *Adv. Mater.* **2012**, *24*, 5832–5836.
190. Perea-López, N.; Elías, A. L.; Berkdemir, A.; Castro-Beltran, A.; Gutiérrez, H. R.; Feng, S.; Lv, R.; Hayashi, T.; López-Urías, F.; Ghosh, S.; *et al.* Photosensor Device Based on Few-Layered WS_2 Films. *Adv. Funct. Mater.* **2013**, *23*, 5511–5517.
191. Lee, H. S.; Min, S.-W.; Chang, Y.-G.; Park, M. K.; Nam, T.; Kim, H.; Kim, J. H.; Ryu, S.; Im, S. MoS_2 Nanosheet Phototransistors with Thickness-Modulated Optical Energy Gap. *Nano Lett.* **2012**, *12*, 3695–3700.
192. Allen, J. E.; Hemesath, E. R.; Lauhon, L. J. Scanning Photocurrent Microscopy Analysis of Si Nanowire

Field-Effect Transistors Fabricated by Surface Etching of the Channel. *Nano Lett.* **2009**, *9*, 1903–1908.
193. Gu, Y.; Kwak, E. S.; Lensch, J. L.; Allen, J. E.; Odom, T. W.; Lauhon, L. J. Near-Field Scanning Photocurrent Microscopy of a Nanowire Photodetector. *Appl. Phys. Lett.* **2005**, *87*, 043111.
194. Wu, C.-C.; Jariwala, D.; Sangwan, V. K.; Marks, T. J.; Hersam, M. C.; Lauhon, L. J. Elucidating the Photoresponse of Ultrathin MoS_2 Field-Effect Transistors by Scanning Photocurrent Microscopy. *J. Phys. Chem. Lett.* **2013**, *4*, 2508–2513.
195. Lopez-Sanchez, O.; Lembke, D.; Kayci, M.; Radenovic, A.; Kis, A. Ultrasensitive Photodetectors Based on Monolayer MoS_2. *Nat. Nanotechnol.* **2013**, *8*, 497–501.
196. Roy, K.; Padmanabhan, M.; Goswami, S.; Sai, T. P.; Ramalingam, G.; Raghavan, S.; Ghosh, A. Graphene–MoS_2 Hybrid Structures for Multifunctional Photoresponsive Memory Devices. *Nat. Nanotechnol.* **2013**, *8*, 826–830.
197. Zhang, W.; Chuu, C.-P.; Huang, J.-K.; Chen, C.-H.; Tsai, M.-L.; Chang, Y.-H.; Liang, C.-T.; He, H., Jr.; Chou, M.-Y.; Li, L.-J. Ultrahigh-Gain Photodetectors Based on Atomically Thin Graphene–MoS_2 Heterostructures. *Sci. Rep.* **2013**, *4*, 3826.
198. Konstantatos, G.; Badioli, M.; Gaudreau, L.; Osmond, J.; Bernechea, M.; de Arquer, F. P. G.; Gatti, F.; Koppens, F. H. Hybrid Graphene–Quantum Dot Phototransistors with Ultrahigh Gain. *Nat. Nanotechnol.* **2012**, *7*, 363–368.
199. Sze, S. M.; Ng, K. K. *Physics of Semiconductor Devices*, 3rd ed.; Wiley: New York, 2007.
200. Tsai, D.-S.; Lien, D.-H.; Tsai, M.-L.; Su, S.-H.; Chen, K.-M.; Ke, J., Jr.; Yu, Y.-C.; Li, L.-J.; He, H., Jr. Trilayered MoS_2 Metal–Semiconductor–Metal Photodetectors: Photogain and Radiation Resistance. *IEEE J. Sel. Top. Quantum Electron.* **2014**, *20*, 3800206.
201. Tsai, D.-S.; Liu, K.-K.; Lien, D.-H.; Tsai, M.-L.; Kang, C.-F.; Lin, C.-A.; Li, L.-J.; He, J.-H. Few Layer MoS_2 with Broadband High Photogain and Fast Optical Switching for Use in Harsh Environments. *ACS Nano* **2013**, *7*, 3905–3911.
202. Yu, W. J.; Liu, Y.; Zhou, H.; Yin, A.; Li, Z.; Huang, Y.; Duan, X. Highly Efficient Gate-Tunable Photocurrent Generation in Vertical Heterostructures of Layered Materials. *Nat. Nanotechnol.* **2013**, *8*, 952–958.
203. Ye, Y.; Ye, Z.; Gharghi, M.; Zhu, H.; Zhao, M.; Yin, X.; Zhang, X. Exciton-Related Electroluminescence from Monolayer MoS_2. *arXiv:1305.4235* **2013**.
204. Esmaeili-Rad, M. R.; Salahuddin, S. High Performance Molybdenum Disulfide Amorphous Silicon Heterojunction Photodetector. *Sci. Rep.* **2013**, *3*, 2345.
205. Bernardi, M.; Palummo, M.; Grossman, J. C. Extraordinary Sunlight Absorption and One Nanometer Thick Photovoltaics Using Two-Dimensional Monolayer Materials. *Nano Lett.* **2013**, *13*, 3664–3670.
206. Fontana, M.; Deppe, T.; Boyd, A. K.; Rinzan, M.; Liu, A. Y.; Paranjape, M.; Barbara, P. Electron–Hole Transport and Photovoltaic Effect in Gated MoS_2 Schottky Junctions. *Sci. Rep.* **2013**, *3*, 1634.
207. Pospischil, A.; Furchi, M. M.; Mueller, T. Solar Energy Conversion and Light Emission in an Atomic Monolayer p-n Diode. *arXiv:1309.7492* **2013**.
208. Britnell, L.; Ribeiro, R.; Eckmann, A.; Jalil, R.; Belle, B.; Mishchenko, A.; Kim, Y.-J.; Gorbachev, R.; Georgiou, T.; Morozov, S.; *et al.* Strong Light–Matter Interactions in Heterostructures of Atomically Thin Films. *Science* **2013**, *340*, 1311–1314.
209. Eda, G.; Maier, S. A. Two-Dimensional Crystals: Managing Light for Optoelectronics. *ACS Nano* **2013**, *7*, 5660–5665.
210. Lin, J.; Li, H.; Zhang, H.; Chen, W. Plasmonic Enhancement of Photocurrent in MoS_2 Field-Effect-Transistor. *Appl. Phys. Lett.* **2013**, *102*, 203109.
211. Feng, J.; Qian, X.; Huang, C.-W.; Li, J. Strain-Engineered Artificial Atom as a Broad-Spectrum Solar Energy Funnel. *Nat. Photonics* **2012**, *6*, 866–872.
212. Sundaram, R.; Engel, M.; Lombardo, A.; Krupke, R.; Ferrari, A.; Avouris, P.; Steiner, M. Electroluminescence in Single Layer MoS_2. *Nano Lett.* **2013**, *13*, 1416–1421.
213. Baugher, B. W.; Churchill, H. O.; Yafang, Y.; Jarillo-Herrero, P. Electrically Tunable p-n Diodes in a Monolayer Dichalcogenide. *arXiv:1310.0452* **2013**.
214. Ross, J. S.; Klement, P.; Jones, A. M.; Ghimire, N. J.; Yan, J.; Mandrus, D.; Taniguchi, T.; Watanabe, K.; Kitamura, K.; Yao, W.; *et al.* Electrically Tunable Excitonic Light Emitting Diodes Based on Monolayer WSe_2 p-n Junctions. *arXiv:1312.1435* **2013**.
215. Li, H.; Yin, Z.; He, Q.; Li, H.; Huang, X.; Lu, G.; Fam, D. W. H.; Tok, A. I. Y.; Zhang, Q.; Zhang, H. Fabrication of Single-and Multilayer MoS_2 Film-Based Field-Effect Transistors for Sensing NO at Room Temperature. *Small* **2012**, *8*, 63–67.
216. Late, D. J.; Huang, Y.-K.; Liu, B.; Acharya, J.; Shirodkar, S. N.; Luo, J.; Yan, A.; Charles, D.; Waghmare, U. V.; Dravid, V. P.; *et al.* Sensing Behavior of Atomically Thin-Layered MoS_2 Transistors. *ACS Nano* **2013**, *7*, 4879–4891.
217. Perkins, F. K.; Friedman, A. L.; Cobas, E.; Campbell, P. M.; Jernigan, G. G.; Jonker, B. T. Chemical Vapor Sensing with Monolayer MoS_2. *Nano Lett.* **2013**, *13*, 668–673.
218. Lee, K.; Gatensby, R.; McEvoy, N.; Hallam, T.; Duesberg, G. S. High Performance Sensors Based on Molybdenum Disulfide Thin Films. *Adv. Mater.* **2013**, *25*, 6699–6702.
219. He, Q.; Zeng, Z.; Yin, Z.; Li, H.; Wu, S.; Huang, X.; Zhang, H. Fabrication of Flexible MoS_2 Thin-Film Transistor Arrays for Practical Gas-Sensing Applications. *Small* **2012**, *8*, 2994–2999.
220. Wu, S.; Zeng, Z.; He, Q.; Wang, Z.; Wang, S. J.; Du, Y.; Yin, Z.; Sun, X.; Chen, W.; Zhang, H. Electrochemically Reduced Single-Layer MoS_2 Nanosheets: Characterization, Properties, and Sensing Applications. *Small* **2012**, *8*, 2264–2270.
221. Zhu, C.; Zeng, Z.; Li, H.; Li, F.; Fan, C.; Zhang, H. Single-Layer MoS_2-Based Nanoprobes for Homogeneous Detection of Biomolecules. *J. Am. Chem. Soc.* **2013**, *135*, 5998–6001.
222. Tongay, S.; Zhou, J.; Ataca, C.; Liu, J.; Kang, J. S.; Matthews, T. S.; You, L.; Li, J.; Grossman, J. C.; Wu, J. Broad-Range Modulation of Light Emission in Two-Dimensional Semiconductors by Molecular Physisorption Gating. *Nano Lett.* **2013**, *13*, 2831–2836.
223. Hui, Y. Y.; Liu, X.; Jie, W.; Chan, N. Y.; Hao, J.; Hsu, Y.-T.; Li, L.-J.; Guo, W.; Lau, S. P. Exceptional Tunability of Band Energy in a Compressively Strained Trilayer MoS_2 Sheet. *ACS Nano* **2013**, *7*, 7126–7131.